DIGITAL COMPENSATION OF THE THRUST
VECTOR CONTROL SYSTEM

Prepared By

SAMPLED-DATA CONTROL SYSTEMS GROUP
AUBURN UNIVERSITY
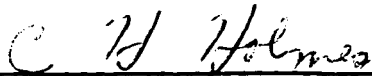
C. L. PHILLIPS, TECHNICAL DIRECTOR

FOURTH TECHNICAL REPORT

28 SEPTEMBER 1965 TO 28 JANUARY 1966

CONTRACT NAS8-11274

GEORGE C. MARSHALL SPACE FLIGHT CENTER
NATIONAL AERONAUTICS AND SPACE ADMINISTRATION
HUNTSVILLE, ALABAMA

APPROVED BY: SUBMITTED BY:

C. H. Holmes   H. M. Summer
Head Professor   Professor of
Electrical Engineering   Electrical Engineering

TABLE OF CONTENTS

LIST OF FIGURES

LIST OF TABLES

LIST OF SYMBOLS

C	System output
G1BN	Bending mode transfer function in attitude channel
G1R	Rigid body transfer function in attitude channel
G2BN	Bending mode transfer function in attitude rate channel
$G_c(z)$	Discrete data compensation transfer function in $\dot{\phi}$ channel
H_o	Zero-order hold transfer function
PHDTCO	Continuous data compensation transfer function in $\dot{\phi}$ channel
R	System input
T	Sampling period, seconds
W_{ss}	Control engine transfer function
β_c	Engine command signal
β_e	Continuous control engine deflection angle, degrees
ϕ	Attitude error signal
$\dot{\phi}$	Attitude rate error
ω_s	Sampling frequency, radians per second
*	Sampled signal

FOREWORD

This report is a technical summary of the progress made since
September 28, 1965 by the Electrical Engineering Department, Auburn
University toward fulfillment of Contract No. NAS8-11274 granted to
Auburn Research Foundation, Auburn, Alabama. The contract was awarded
May 28, 1964 by the George C. Marshall Space Flight Center, National
Aeronautics and Space Administration, Huntsville, Alabama.

SUMMARY

A discussion of an exact method for the determination of stability margins in any channel of a multiloop sampled data system is given. The stability margins are determined for the attitude channel of the thrust vector control system using a continuous compensation function and a 2.5 hertz sampling rate. A design approach is suggested for the development of digital compensation in the attitude rate channel and examples are given for 25 hertz and 2.5 hertz system sampling rates. The "hidden instability" problem is discussed and general guidelines are given for the prevention of system instability. An introduction to the analysis of multirate sampling systems is presented and several methods of analysis are investigated.

PERSONNEL

The following named staff members of Auburn University have actively participated on this project.

C. L. Phillips - Professor of Electrical Engineering

H. M. Summer - Professor of Electrical Engineering

G. T. Nichols - Professor of Electrical Engineering

C. C. Carroll - Associate Professor of Electrical Engineering

R. K. Cavin, III- Graduate Assistant in Electrical Engineering

I. INTRODUCTION

In the "Third Technical Report" considerable emphasis was placed on approximate methods for determining an open-loop transfer function for a multiloop sampled-data system opened between continuous data elements. This transfer function is required to facilitate compensation of the system using standard frequency domain techniques and to provide a method of ascertaining stability margins. Although a procedure for obtaining an exact transfer function is not known, and may not exist, the exact stability margins may be determined at any point by the approach suggested in Chapter II.

Chapter III contains the results of a brief investigation into the effect of a reduced sampling rate on the stability of the configuration described by Figure 1.

The design of a digitally-compensated control system is discussed in Chapter IV. A design technique is evolved and applied to the development of a compensation function for the case when the sampling rate is 25 hertz and again when the system sampling rate is 2.5 hertz.

It is reasonable to expect that system performance may be enhanced by using different rates of sampling in the rate and attitude loops. Chapter V, which serves as an introduction into the area of multiloop systems, summarizes the findings in this field to date.

1
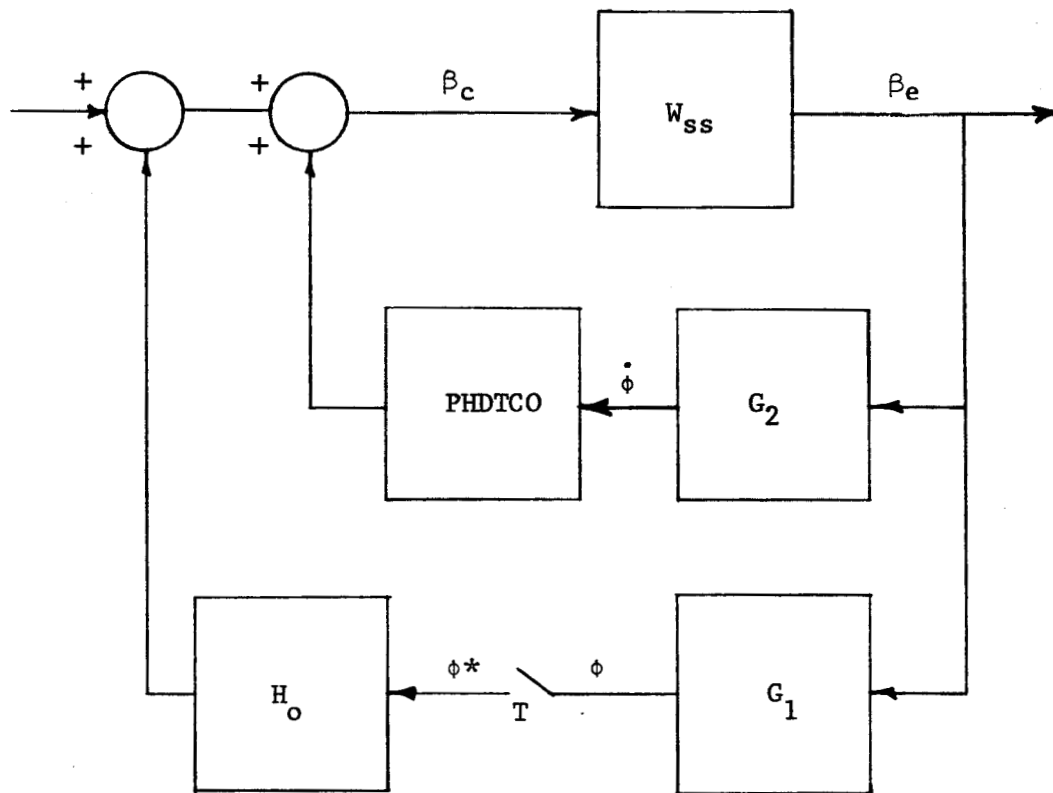
Fig. 1--Block diagram of the thrust vector control system.

II. THE EXACT METHOD FOR DETERMINATION OF STABILITY MARGINS

R. Cavin, III

For a combined analog-sampled system such as the thrust vector

control system of Figure 1, it is often necessary to obtain infor-

mation indicative of system stability margin for various branches of

the block diagram. Two of the most common and most useful measures

of system stability are gain margin and phase margin, both of which

result from frequency dependent stability criteria. In order to

obtain gain and phase margin, it is normally necessary to develop

an open loop transfer function at that point in the system where

stability margins are desired. As has been illustrated in previous

reports[1], an exact open loop transfer function cannot presently be

written for a multiloop combined analog-sampled system, opened between

continuous elements. In fact for the particular system of Figure 1,

an exact, sampled, open loop transfer characteristic can only be

determined by opening the system at ϕ. Of course, Nyquist plots

derived from this open loop transfer characteristic can be used to:

(a) give exact phase and gain margin at ϕ and (b) determine whether

or not a pratical combination of parameters and compensation yield

a stable system.

---

[1]Phillips, C.L., et.al., "Digital Compensation of the Thrust Vector
Control System" Second Technical Report Auburn Research Foundation,
1 November 1964 to 28 May 1964, page 5.

Now the "exact method", discussed in the STL Interim Report
4185-6005-RU000, section II-B-3-a[2], takes advantage of the available
open-loop transfer characteristic at ϕ in order to determine the
gain margin at any other point in the system. For instance the gain
margin at β_c can be determined by inserting a variable gain at β_c,
increasing (or decreasing) this gain from unity until the open loop
Nyquist at ϕ indicates that the system is unstable. The gain margin
at β_c then is simply that value of gain at which neutral stability
is effected.

Although not discussed in the referenced STL report, the phase
margin at any point in the system may be determined in much the same
manner. The phase margin at β_c, for example, can be determined by
inserting a phase shift term, $e^{j\theta}$, at β_c and varying θ positively (or
negatively) about zero until the open loop Nyquist at ϕ indicates
system instability. That value of θ which causes neutral stability
is the phase margin of the system at β_c. One of the biggest short-
comings of the exact method is that convergence to the stability
margin is not always systematic. A plot such as that of Figure 2-9
of the referenced STL report, where gain margin at ϕ is plotted as
a function of gain at β_c, should increase the rate at which one
converges to the gain margin at β_c.

Another disadvantage of the "exact method" is that for each
value of gain or phase at the branch under investigation, a new

---

[2] J. Holzmon, et al, "Review of Digital Control System Design Techniques
for Missiles", STL Report 4185-6005-RU000, 16 April, 1965.

Nyquist plot at φ must be generated. Further, if the system, is unstable,

little information can be derived from the exact method that will

aid in the choice of suitable compensation, i.e., the open loop

frequency response at the branch under study is not available by the

"exact method". This method is therefore limited to the determina-

tion of system stability margins and, in general, is not well suited

for the synthesis problem.

It should be emphasized that the variation of gain or phase shift

at β_c will alter the location of the open loop poles for the φ trans-

fer function and consequently may change the required number of en-

circlements of the -1 point by the φ-Nyquist plot to give stable

operation. However, rather than attempt to extract the closed-inner

loop roots for each value of θ or gain, a much more tractable approach

is provided by plotting a Nyquist diagram for the inner loop alone,

opened at β_c. Then, if the open-loop roots of the inner loop transfer

function are known, the effect of gain or phase shift at β_c on closed

inner-loop roots and therefore roots of the open-loop transfer func-

tion for φ can be directly determined. The above method can best be

illustrated by an example. Consider the simple system of Figure 2.

(1) First, construct a Nyquist diagram of inner loop with K = 1.

This is given by Figure 3. There is one unstable open loop root and

no net encirclements of -1 point; thus, there is one unstable closed-

loop pole. If K is greater than 2, there are no unstable closed-
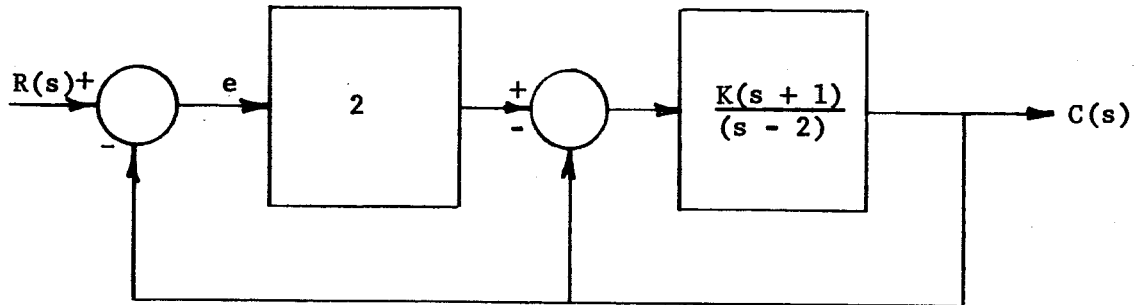
Fig. 2--Example system.
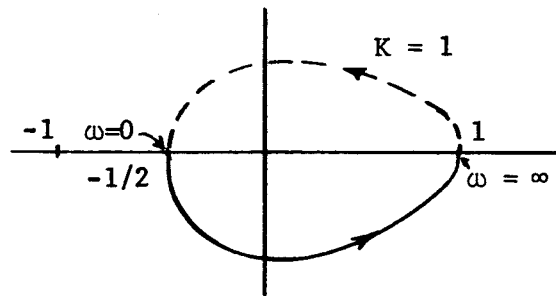
Fig. 3--Inner loop Nyquist plot for the example system.

loop poles. (The Nyquist diagram need not be replotted for each K:
rather, the effect of K variation can be shown by changing the scale
of the plot.)

(2) Next construct the outer loop Nyquist diagram for the
system for different values of K. Choose K = 1. The form of the
Nyquist is given by Figure 4. There is one net encirclement of the
-1 point, and since, from Figure 3 there is one unstable open loop
root, the system is stable.

(3) Consider the outer loop Nyquist diagram for K = 3 as given
by Figure 5. Note that there are no encirclements of -1. However,
from Figure 3 there are no unstable open loop roots, thus the system
is stable.

The above example, while elementary from the standpoint of mathe-
matical complexity, does serve to emphasize the necessity of main-
taining a systematic method to keep track of the open loop roots of
the system.
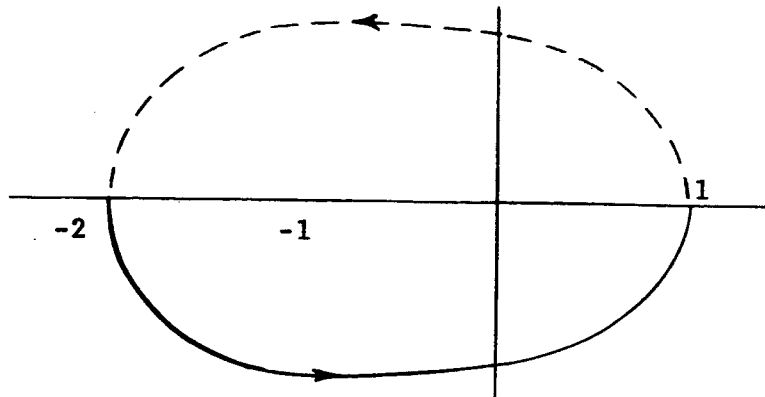
Fig. 4--Outer loop Nyquist plot for the example system with K = 1. (Inner loop closed.)
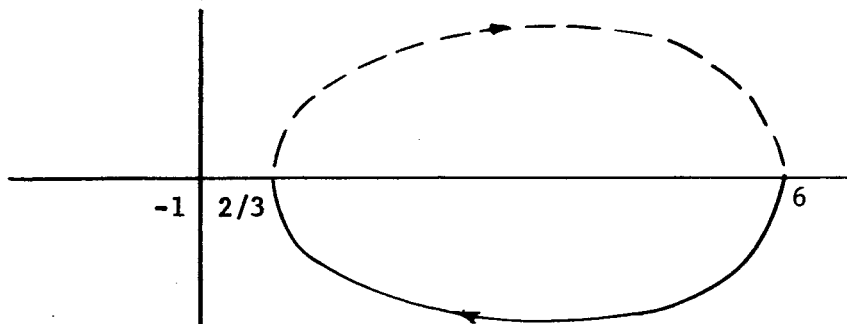
Fig. 5--Outer loop Nyquist plot for example system with K = 3. (Inner loop closed.)

III. STABILITY OF THE THRUST VECTOR CONTROL SYSTEM WITH A 2.5 HERTZ SAMPLING RATE

R. Cavin, III

In order to determine the effect of reduced sampling frequency on system stability, the system described by Figure 1 and the equations of Appendix A was investigated for a sampling frequency of 2.5 hertz. An open loop transfer function can be developed only at ϕ when this sampling frequency is used. This limitation results because the continuous-data and fictitious sampler approximation methods are not applicable when $\omega_s/2$ is in the range of the bending mode frequencies. (ω_s denotes the system sampling frequency.) Consequently, it is only possible to compare the Nyquist diagrams of the 2.5 hertz system and the 25 hertz systems by using the open loop transfer functions computed at ϕ. These Nyquist diagrams were developed with the aid of the computer program of Appendix B.

Figure 6 is a Nyquist diagram for the system of Figure 1 opened at ϕ with $a_0 = a_1 = 0.5$ and $T = 0.4$ seconds. Note that the system has a rigid body gain margin of 8 db and a phase margin of -25 degrees. Because of the increased attenuation of the 2.5 hertz zero-order hold relative to the 25 hertz zero-order hold at the body bending frequencies, the body bending modes do not present a serious stability problem. Figure 7 is a Nyquist diagram for the system of Figure 1 opened at ϕ with $a_0 = a_1 = 0.5$ and $T = 0.04$ seconds. For this fast
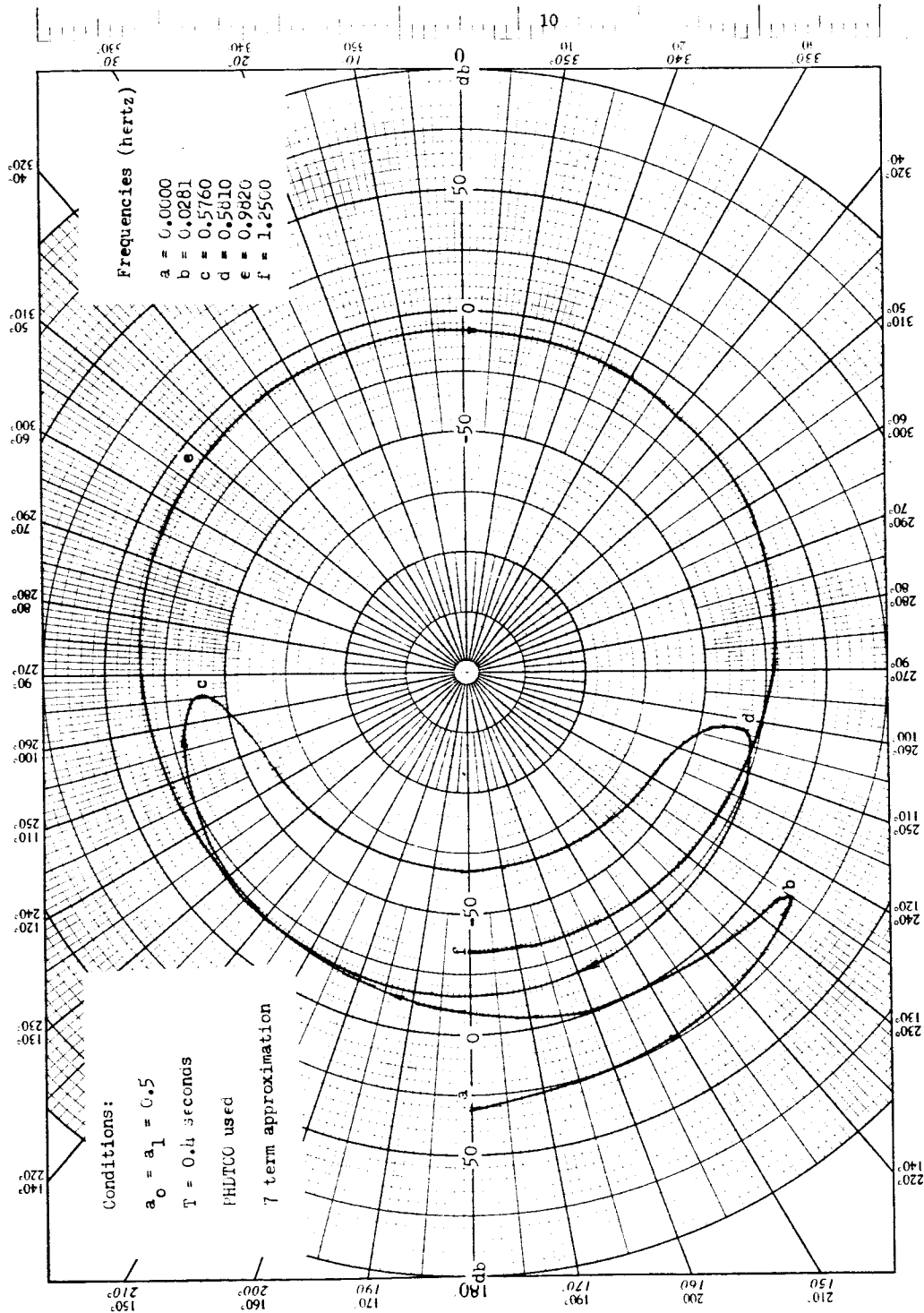
Fig. 6—Nyquist diagram of thrust vector control system of Figure 1 broken in Φ channel.
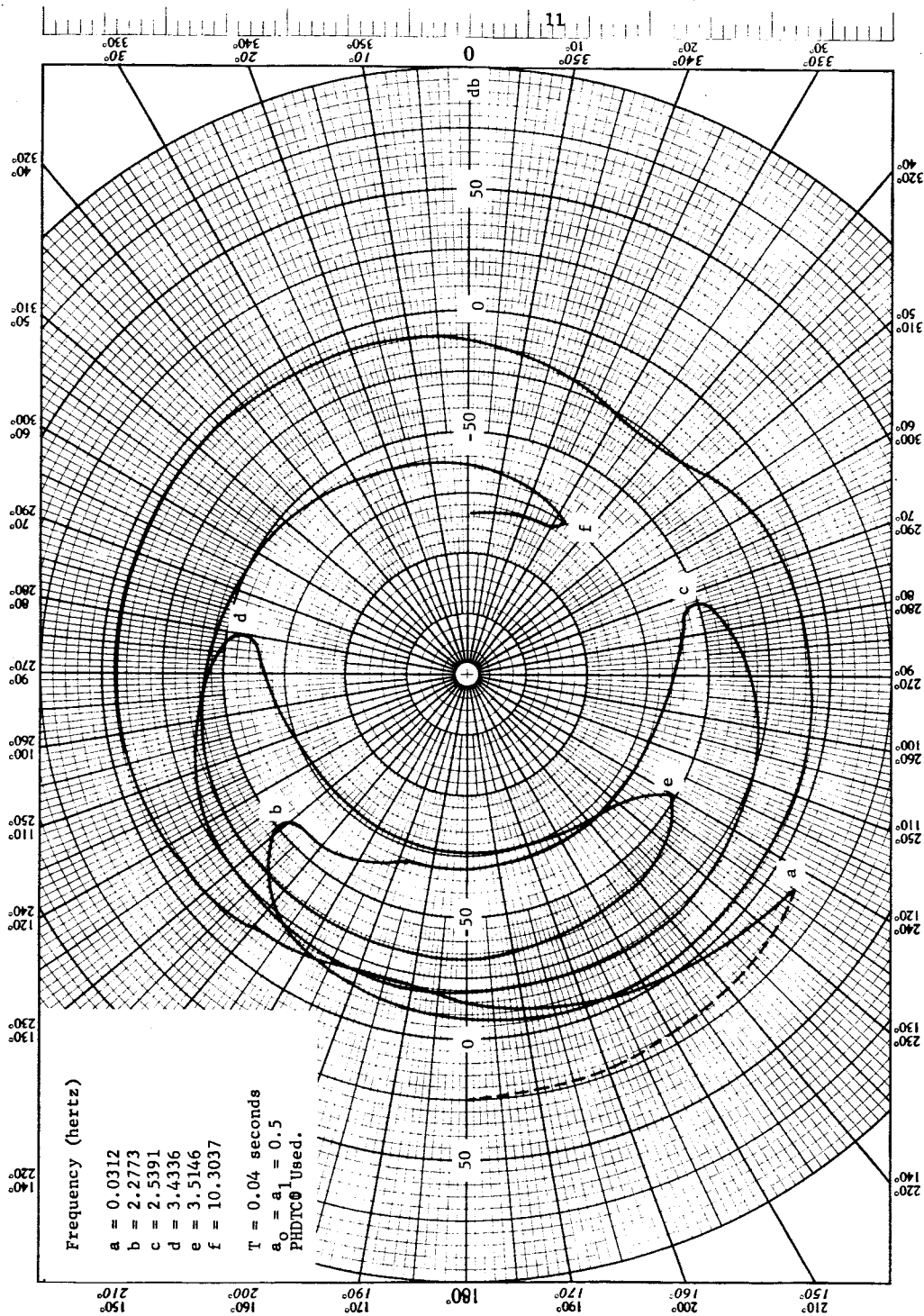
Fig. 7--Nyquist diagram of thrust vector control system of Figure 1 opened in φ channel.

Frequency (hertz)

a = 0.0312
b = 2.2773
c = 2.5391
d = 3.4336
e = 3.5146
f = 10.3037

T = 0.04 seconds
$a_o = a_1 = 0.5$
PHDTCO Used.

rate system, a phase margin of -36° and a rigid body gain margin of 16 db are provided by the compensation function, PHDTC0. However, the second bending mode has a gain margin of only +9 db.

Consequently, for the example chosen, the reduced sampling rate diminishes rigid body stability margins relative to those of the same system with fast-rate sampling and provides increased bending mode stability margins relative to those of the fast-rate system. The reduction of rigid body stability margins is due primarily to the phase lag introduced by the zero-order hold.

IV. THE DESIGN OF A DIGITALLY COMPENSATED
THRUST VECTOR CONTROL SYSTEM

R. Cavin,III

Introduction

In this chapter, a method for determining digital compensation
for the thrust vector control system is developed. The design pro-
cedure is illustrated by the development of compensation functions
for a 25 hertz and a 2.5 hertz sampling rate system. General dis-
cussions are given on the problem of hidden instability in sampled-
data control systems.

The assumptions which are pertinent to the design approach taken
in this chapter are:

1. The vehicle attitude and attitude rate will be assumed to be
   synchronously sampled at the same sampling frequency.

2. When the required digital compensation transfer functions are
   determined, a vehicle digital computer is assumed to be
   available to implement the specified digital transfer func-
   tions.

3. Design factors other than stability, such as load relief,
   are not considered.

Some Analytical Considerations

A useful characteristic of sampled data systems is that the fre-
quency response, whether determined in the z, s or w plane, is unique.

13

Now, for high order, low-pass systems, it has been found through experience that the frequency response is most easily obtained by the finite series expansion method in the s-plane. For a specified s-plane frequency, $j\omega$, there corresponds a w-plane frequency, jr. jr may be related to $j\omega$ as follows.

$$s = (0 + j\omega) \tag{1}$$

$$z = \frac{1 + w}{1 - w} = e^{Ts} = e^{jT\omega} \tag{2}$$

The solution of equation 2 for w is

$$w = (0 + jr) = \frac{j \sin T\omega}{1 + \cos T\omega} \tag{3}$$

where T is the sampling period.

Therefore, if the open loop frequency response is computed, conventional compensation techniques may be used to specify the w-plane transfer function required for stability. Then by using transformation (1), the required sampled transfer characteristic can be determined.

The development of a compensation function for a digital system follows essentially the same design procedures as that of conventional continuous-data compensation. There are, however, certain aspects of the design process which differ sufficiently to require special consideration. Consider the system block diagram given by Figure 8.

Now, the transfer function for the system shown by Figure 8 is given by equation (4) below.

$$\frac{E_o{}^*}{E_i{}^*}(s) = \frac{\left[H_o AC(s) \right]^*}{1 - \left[H_o AB(s) \right]^*} \tag{4}$$

Suppose that transfer functions B(s) and C(s) have the same poles. (This supposition is applicable for the thrust vector control system since the $\dot{\phi}/\beta_e$ and the ϕ/β_e transfer functions have identical denomitors.) From standard references[1], the starred transform of a function of s, E*(s), is given by equation (5).

$$E^*(s) = \sum_{n=1}^{k} \frac{N(\zeta_n)}{D'(\zeta_n)} \frac{1}{1 - e^{T(\zeta_n - s)}} \tag{5}$$

where: ζ_n designates the nth root of the denominator polynomial, D(s).

k represents the total number of roots of D(s).

$$N(\zeta_n) = N(s) \Big|_{s = \zeta_n}, \quad D(\zeta_n) = D(s) \Big|_{s = \zeta_n}$$

$$D'(\zeta_n) = \frac{dD(\zeta)}{d\zeta} \Big|_{\zeta = \zeta_n}$$

Therefore $\left[H_o AC(s) \right]^*$ and $\left[H_o AB(s) \right]^*$ have identical denominator polynomials in e^{-Ts}, i.e.,

---

[1] Kuo, B.C., Analysis and Synthesis of Sampled-Data Control Systems, (Englewood Cliffs, N. J.: 1963), pp. 54-56.
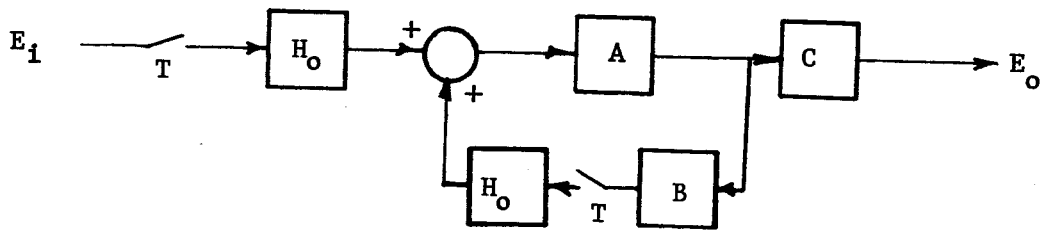
Fig. 8--Block diagram of example system.
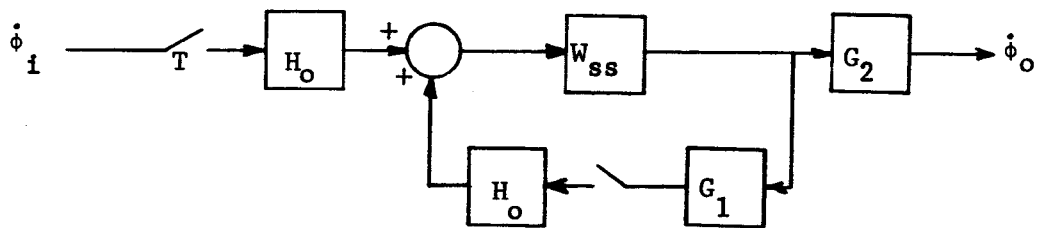
Fig. 9--Block diagram of TVC system opened in $\dot{\phi}$ channel.

$$\left[H_0 AC(s) \right]^* = \frac{P_2}{Q} \quad \text{and} \quad \left[H_0 AB(s) \right]^* = \frac{P_1}{Q} \tag{6}$$

The substitution of (6) into (5) yields:

$$\frac{E_o^*(s)}{E_i^*(s)} = \frac{P_2}{Q - P_1} \tag{7}$$

The usefulness of the result expressed by equation (7) is illustrated in the following paragraph which describes a method of computing the number of unstable poles of the open loop transfer function of the TVC system opened in the $\dot{\phi}$ channel. (See Figure 9)

System transfer functions which are used throughout the report are given by Appendix A. Note that G_1 and G_2 have the same denominators. In order to determine the compensation requirements for the system, a Nyquist diagram can be generated for $(\dot{\phi}_o)^*/(\dot{\phi}_i)^*$. However, before the diagram can be interpreted, it is necessary to know the number of unstable open-loop poles. The number of closed-loop, unstable poles for the closed loop in Figure 9 can be determined by generating a Nyquist plot for this loop alone. Suppose, as an example, that there are two unstable poles due to the closed loop portion of Figure 9 and, as indicated by Appendix A, there is one unstable open-loop pole due to G_2. Because of the cancellation effect described in the preceding paragraphs, there are only two, not three, unstable open-loop poles for the system transfer functions opened in the $\dot{\phi}$ channel.

Compensation Design

In the following paragraphs, the method by which a compensation function can be determined is given. In the ensuing discussion, a sample period of 0.04 seconds is assumed throughout, $a_0 = a_1 = 0.5$, and the transfer functions of Appendix A are used. All Nyquist curves were obtained by using a five term series expansion to represent the starred-transform terms which arise in the open-loop transfer functions and the computer program of Appendix C was used to determine the curves. The following steps were taken to develop the compensation function for the system to be inserted in the $\dot{\phi}$ channel.

A. To determine the total number of open-loop unstable poles for the system opened in the $\dot{\phi}$ channel, it is first necessary to establish the number of open-loop unstable poles contributed by the closed ϕ loop. This can be done by simply generating a Nyquist plot for the ϕ loop alone. The resulting curve is shown by Figure 10. Since the open loop transfer function for the ϕ channel alone contains one unstable pole, there are two unstable poles due to the closed ϕ loop in the open loop transfer function for the system opened in the $\dot{\phi}$ channel. As a consequence of preceding discussions, there are therefore two unstable open-loop poles for the system opened in the $\dot{\phi}$ channel.

B. Next, the total Nyquist plot is generated for the system opened in the $\dot{\phi}$ channel. The open-loop transfer function is given by (8).

Fig. 10--Nyquist plot for φ loop alone.
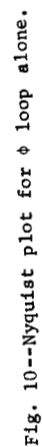
$$O.L.T.F.(\dot\phi) = \frac{(H_o \cdot W_{ss} \cdot G_2)^*}{1.0 - (H_o \cdot W_{ss} \cdot G_1)^*} \tag{8}$$

The resulting Nyquist Curve is given by Figure 11 and indicates that the system characteristic equation has two unstable roots, hence requiring compensation.

C. In order to attain the required two counter-clockwise encirclements on Figure 11, the following design procedure was used. Note that the curve (at low frequency) exceeds zero db at approximately 92 degrees and proceeds in a counter-clockwise sense to -96°, at which point it reverses its direction and crosses the 180 degree line at 17 db. If this 180 degree crossover point is made to occur at less than zero db without altering the remainder of the plot appreciably, stable operation will result. By trial and error, it was determined that the introduction of a double order lag at a w-plane frequency of 0.07 would yield the desired 180 degree crossover at about -15 db. However, the additional phase lag introduced by this double order lag resulted in a condition of possible instability due to the first bending mode. In order to circumvent this potential problem area, it was decided to phase stabilize the first bending mode. This was accomplished by the introduction of a second order lead term at a w-plane frequency of (.24) with a damping ratio of 0.25. The remainder of the bending modes are gain stabilized by this compensation function, which for high frequencies provides an attenuation of approximately -21 db. The complete compensation transfer function is:

Fig. 11--Nyquist plot for the uncompensated system opened in the $\dot{\phi}$ channel with the ϕ channel closed.

$$G_c(w) = \frac{\dfrac{w}{(.24)^4} + \dfrac{(2.0)(0.25)w}{0.24} + 1.0}{(\dfrac{w}{.07} + 1)^2} \qquad (9)$$

where

$$w = (p + jr)$$

Gain and phase plots of $G_c(jr)$ are given by Figures 12 and 13 respectively. Figure 14 is a Nyquist plot for compensated system opened in the $\dot{\phi}$ channel. The open loop transfer for Figure 14 is:

$$\text{O.L.T.F. } (\dot{\phi}_c) = \frac{G_c(w) \cdot (H_o \cdot W_{ss} \cdot G_2)^*}{1.0 - (H_o \cdot W_{ss} \cdot G_1)^*} \qquad (10)$$

From Figure 14, it may be seen that the gain margin in the $\dot{\phi}$ channel is -15 db and +25 db and that phase margins of -53° and $+65^o$ are obtained.

D. The results obtained to this point indicate that acceptable stability margins are provided for the $\dot{\phi}$ channel, however, an important question is: "What are the stability margins provided by this compensation function if the system is opened in the ϕ channel?" Consider the block diagram of the thrust vector control system opened in the ϕ channel shown by Figure 15.

$$G_c(w) = \frac{\dfrac{w^2}{(0.24)^2} + \dfrac{2.0(0.25)w}{0.24} + 1.0}{\left[\dfrac{w}{0.07} + 1\right]^2}$$
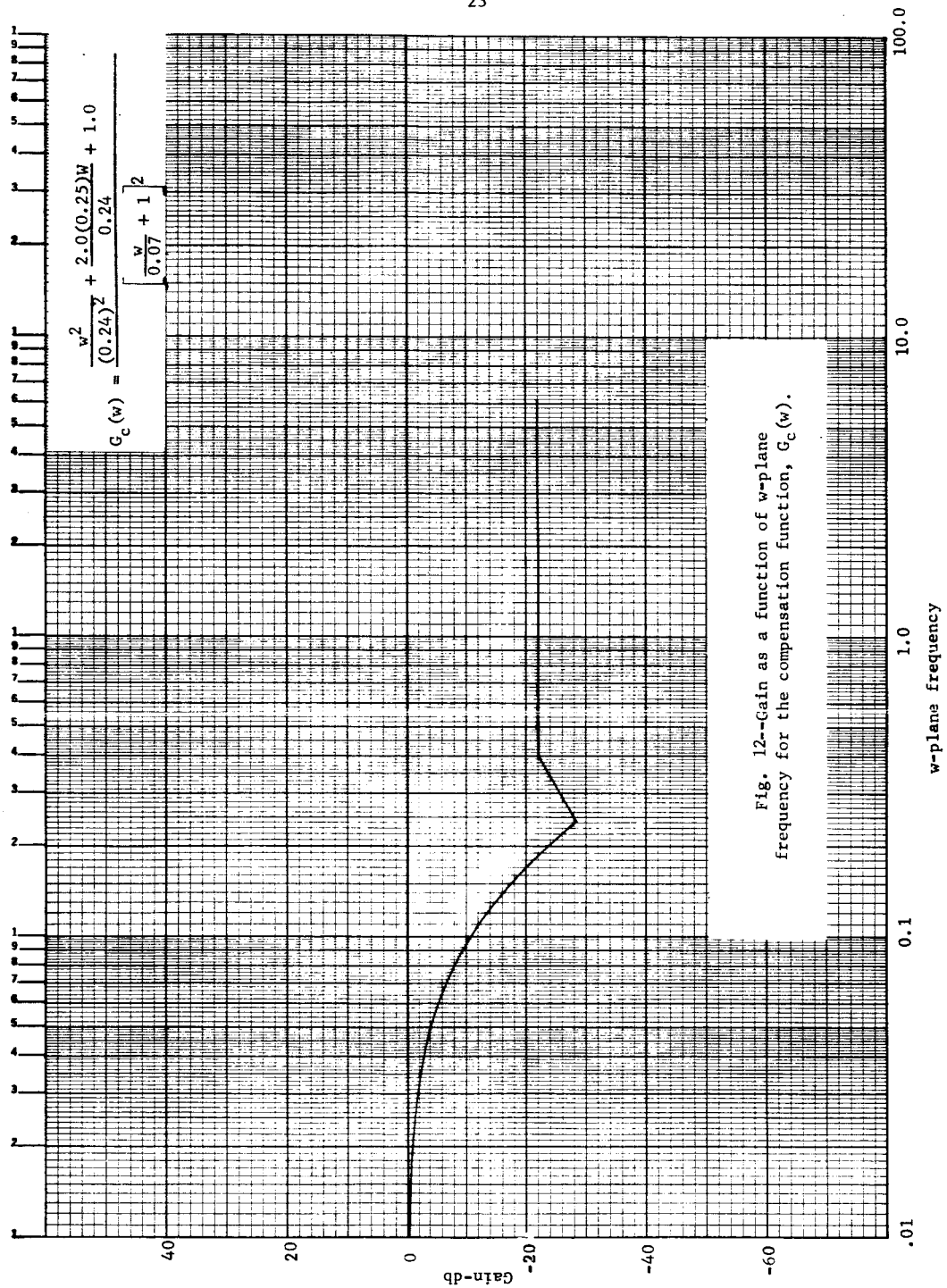
Fig. 12--Gain as a function of w-plane frequency for the compensation function, $G_c(w)$.

Fig. 13--Phase as a function of w-plane
frequency for the compensation function $G_c(w)$.

Frequency-hertz
a = 0.0312
b = 0.1440
c = 1.3315
d = 1.9956
e = 2.5835
f = 3.4604
g = 3.5074
$a_o = a_1 = 0.5$
T = 0.04 seconds
5 term approximation
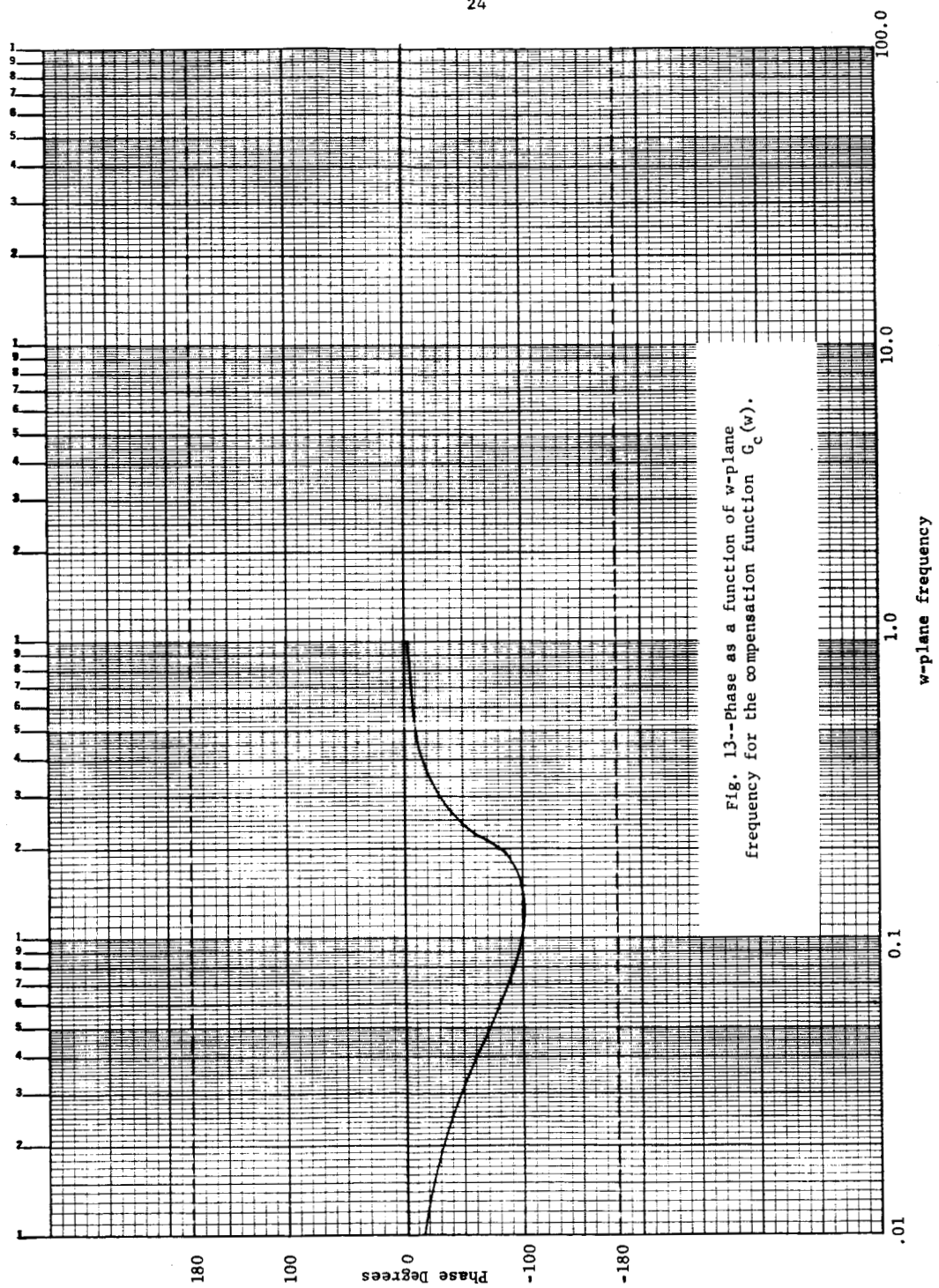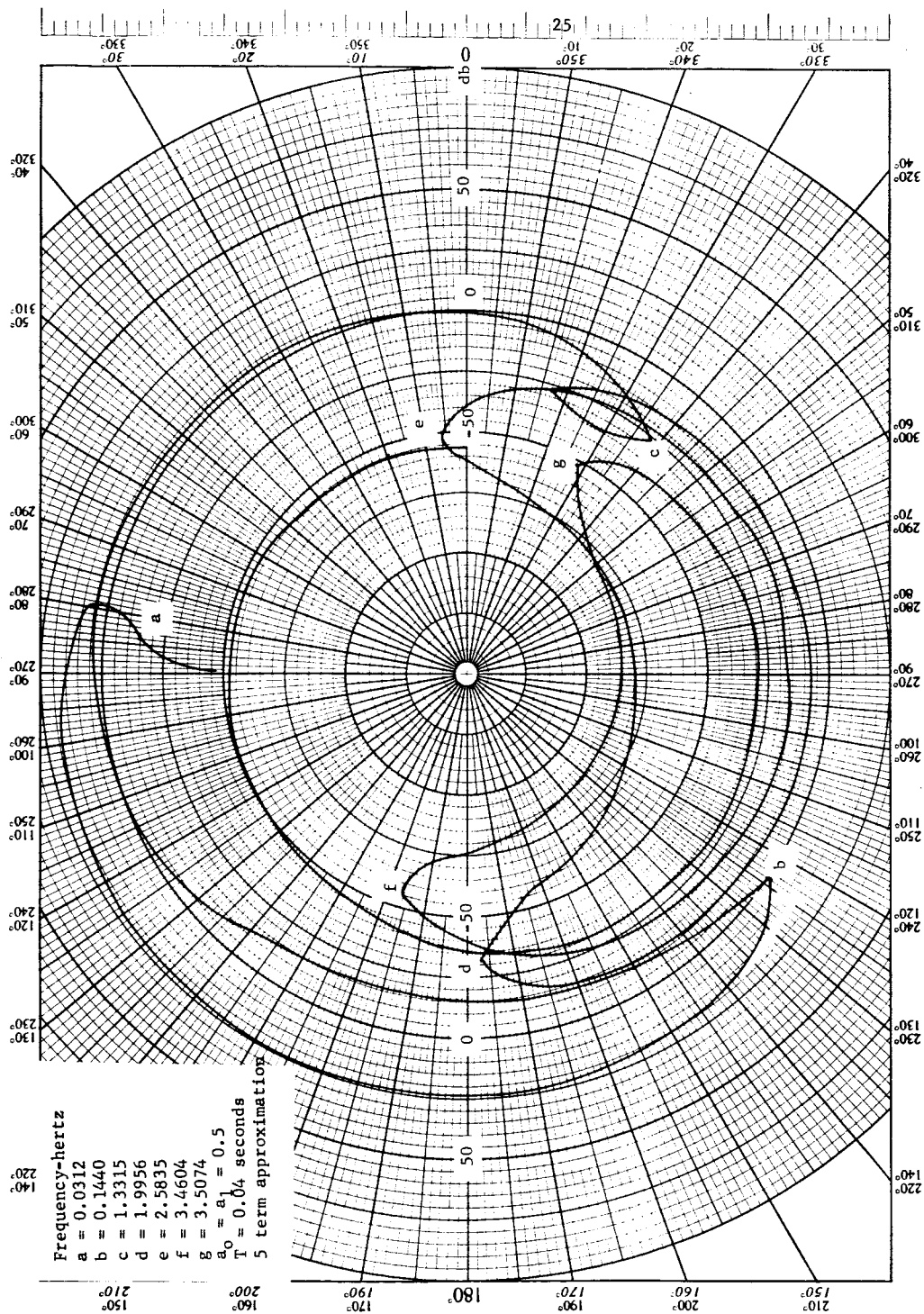
Fig. 14--Nyquist plot for the compensated system opened in the $\dot{\phi}$ loop with the ϕ loop closed.
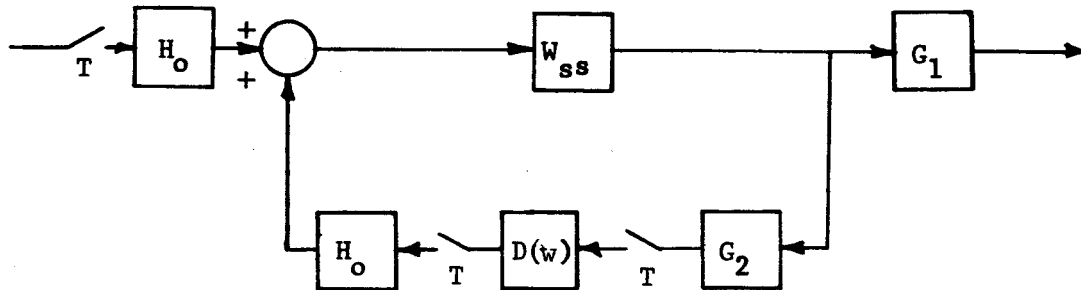
Fig. 15 --Block diagram of compensated thrust vector control
system opened in ϕ channel.

Precisely the same approach which was used in the preceding steps is applicable here. First the number of unstable open-loop poles contributed by the closed, compensated $\dot{\phi}$ loop must be determined. The Nyquist plot for the $\dot{\phi}$ loop alone is given by Figure 16. There is one unstable open loop pole for this loop alone and no net encirclements of -1 point by the Nyquist diagram, thus there is a total of one unstable open-loop roots for the compensated thrust vector control system opened in the ϕ channel.

E. The open-loop transfer function for the system opened in the ϕ channel as shown by Figure 15 is given by equation (11).

$$\text{O.L.T.F.}(\phi_c) = \frac{(H_o \cdot W_{ss} \cdot G_1)^*(s)}{1.0 - G_c(w)(H_o \cdot W_{ss} \cdot G_2)^*(s)} \tag{11}$$

The Nyquist diagram of equation (8) is given by Figure 17. Phase margins of -37 and +80 degrees and gain margins of -8 and -16 db are indicated by Figure 10.

F. A third point in the system at which stability margins are required is β_c. Since $\omega_s/2$ exceeds by almost a factor of four the highest bending mode frequency, acceptably accurate results will be obtained by using the continous approximation method. A block diagram of the system opened at β_c is given by Figure 18, and the open loop transfer function is:

$$\text{O.L.T.F.}(\beta_c) = \frac{W_{ss} G_1 H_o(s)}{T} \left[se^{Ts} + 1 \right] \tag{12}$$

Fig. 16--Nyquist plot for the compensated $\dot{\phi}$ loop alone.

Frequency-hertz

a = 0.0312
b = 1.3408
c = 1.9932
d = 2.5830
e = 3.4619
f = 3.5074
$a_o = a_1 = 0.5$
T = 0.04 seconds
5 Term Approximation

29

Frequency-hertz
a = 0.0312
b = 2.2168
c = 2.5391
d = 3.4316
e = 3.5146
$a_o = a_1 = 0.5$
T = 0.04 seconds
5 Term Approximation
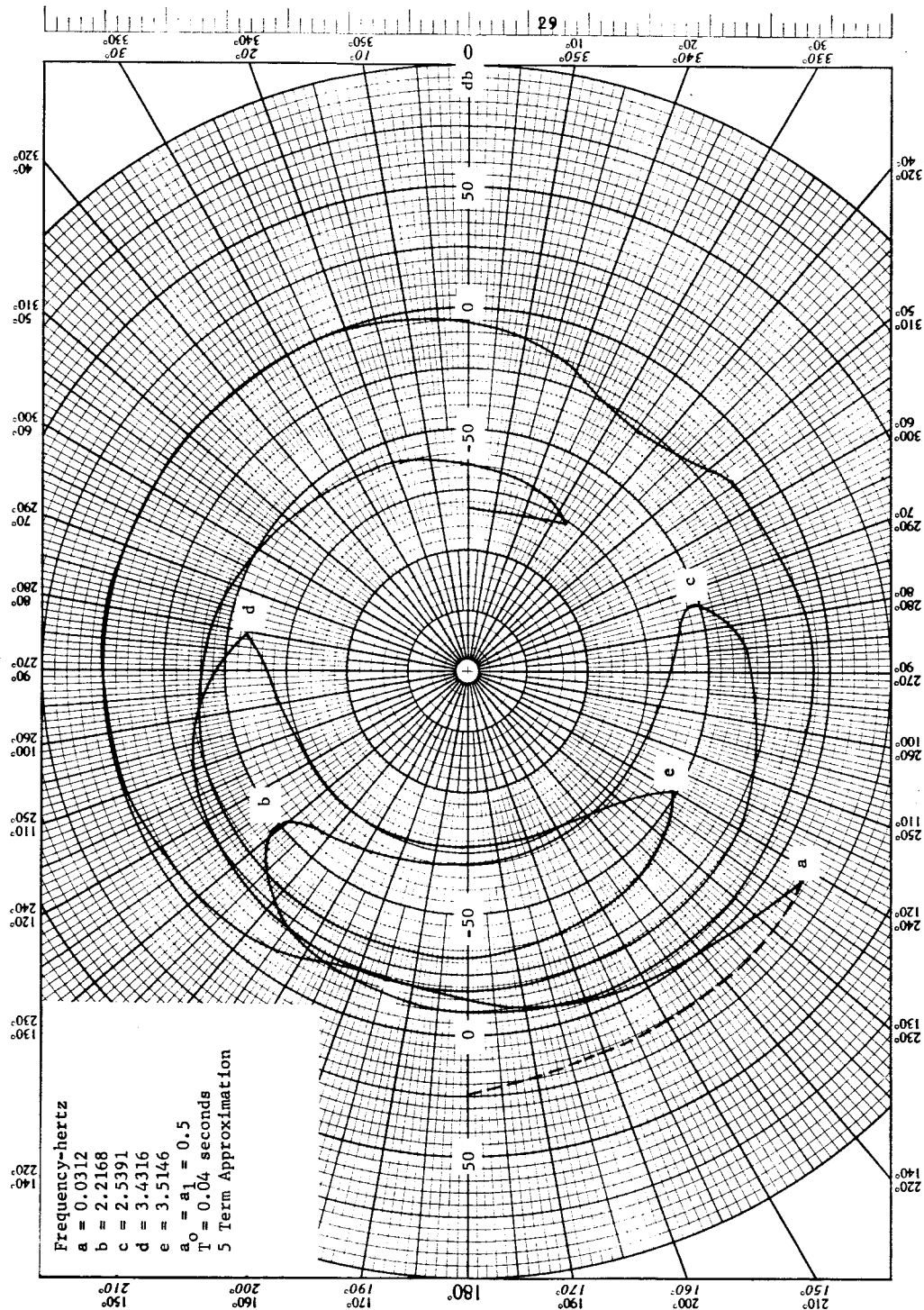
Fig. 17 --Nyquist plot for the compensated system opened in the $\dot{\phi}$ loop with the $\dot{\phi}$ loop closed.
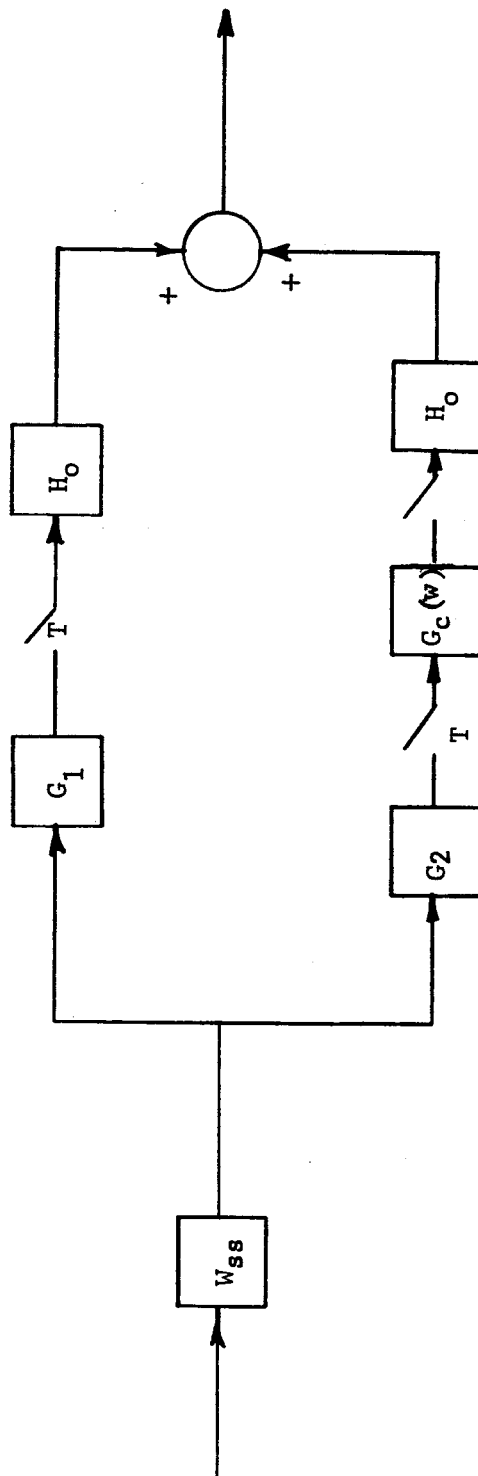
Fig. 18--Block diagram of the compensated thrust vector control system opened at β_c.

Equation 12 indicates that the open-loop transfer function has one unstable root (See Appendix A) and thus one encirclement of the zero db point is required of the Nyquist diagram of the compensated system. Figure 19 is the Nyquist diagram for the system opened at β_c and this figure indicates that the compensation function provides a gain margin of 12 db and a phase margin of -25 degrees.

One potential design difficulty is revealed by Figure 19 in that there is an inordinate amount of loop gain at a phase angle of -150° for the third bending mode frequency. In a production design this would justify refinement of the compensation function given by equation 9.

Realization of the Compensation Function

The z domain transfer function may be computed from (9) by using the transformation given by 13. This is given by equation (14).

$$w = \frac{z - 1}{z + 1} \tag{13}$$

$$G_c(z) = \frac{18.568z - 32.72z + 18.152}{4.2009 \times 10^4 z^2 - 8.3198 \times 10\ z + 4.1193 \times 10^4} = \frac{E_o(z)}{E_i(z)} \tag{14}$$

There are several methods by which the transfer function given by (14) may be realized. In this example the "Direct Programming" method will be used. Dividing the numerator and denominator of (14) by z^2 yields:

Frequency (hertz)

a = 0.1562
b = 2.1338
c = 2.6006
d = 3.4307
e = 3.5146
f = 12,6162

T = 0.04
$a_0 = a_1 = 0.5$
Continuous Approx
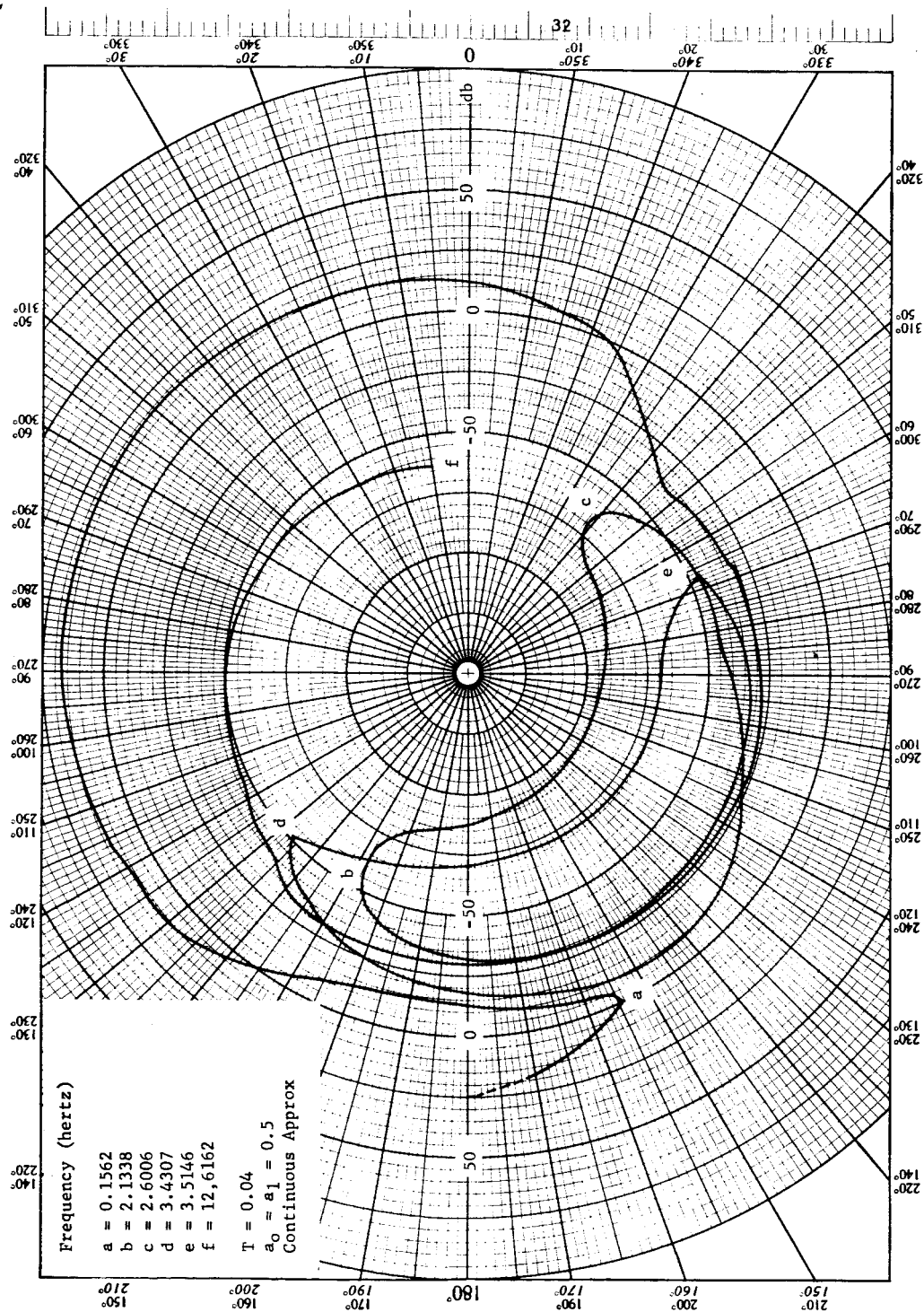
Fig. 19--Nyquist plot for the compensated thrust vector control system opened at β_c.

$$\frac{E_o(z)}{E_i(z)} = \frac{18.568 - 32.72z^{-1} + 18.152z^{-2}}{4.2009 \times 10^4 - 8.3198 \times 10^4 z^{-1} + 4.1193 \times 10^4 z^{-2}} \qquad (15)$$

or equivalently:

$$(4.2009 \times 10^4 - 8.3198 \times 10^{-4} z^{-1} + 4.1193 \times 10^4 z^{-2}) E_o(z) =$$

$$(18.568 - 32.72z^{-1} + 18.152z^{-2}) E_i(z) \qquad (16)$$

Taking the inverse z transform yields:

$$4.2009 \times 10^{+4} e_o{}^*(t) - 8.3198 \times 10^{+4} e_o{}^*(t - T) + 4.1193 \times 10^4 e_o{}^*(t - 2T) =$$

$$18.568 \, e_i{}^*(t) - 32.72 e_i{}^*(t - T) + 18.152 \, e_i{}^*(t - 2T) \qquad (17)$$

Solving equation (17) for $e_o{}^*(t)$ gives:

$$e_o{}^*(t) = \frac{18.568}{4.2009 \times 10^4} e_i{}^*(t) - \frac{32.72}{4.2009 \times 10^4} e_i{}^*(t-T) + \frac{18.152}{4.2009 \times 10^4} e_i{}^*(t-2T)$$

$$+ \left(\frac{8.3198}{4.2009}\right) e_o{}^*(t - T) - \left(\frac{4.1193}{4.2009}\right) e_o{}^*(t - 2T) \qquad (18)$$

For simplicity of notation, let

$$a = \frac{18.568}{4.2009 \times 10^4}, \quad b = \frac{32.72}{4.2009 \times 10^4}, \quad c = \frac{18.152}{4.2009 \times 10^4}, \quad d = \frac{8.3198}{4.2009}$$

$$e = \frac{4.1193}{4.2009}$$

Thus (18) becomes

$$e_o*(t) = ae_i*(t) - be_i*(t-T) + ce_i*(t-2T) + de_o*(t-T)$$

$$(19)$$

$$-e \ e_o*(t-2T)$$

The implementation of equation (19) is given by Figure 20.

Digital Compensation of the Thrust Vector Control System With a Sampling Rate of 2.5 Hertz

In order to determine the effect of a reduced sampling rate on the compensation problem, the stabilization technique applied previously was applied to the thrust vector control system using a sampling rate of 2.5 hertz in both the rate and attitude channels.

The Nyquist diagram for the ϕ loop alone is given by Figure 21. From Figure 21, it is apparent that there are two unstable roots due to the closed ϕ loop. Therefore, there are two unstable poles for the open-loop transfer function at $\dot{\phi}$.

The Nyquist diagram for the uncompensated system opened in the $\dot{\phi}$ channel is presented by Figure 22. Note the rather erratic behavior of this curve. This results from reflected bending modes, and this unusual behavior is particularly evident when the system is opened in the $\dot{\phi}$ channel. A compensation function which results in a stable system was derived by utilizing the Bode plots of Figures 23 and 24 in conjunction with trial and error compensation methods. The compensation is given by equation (20).
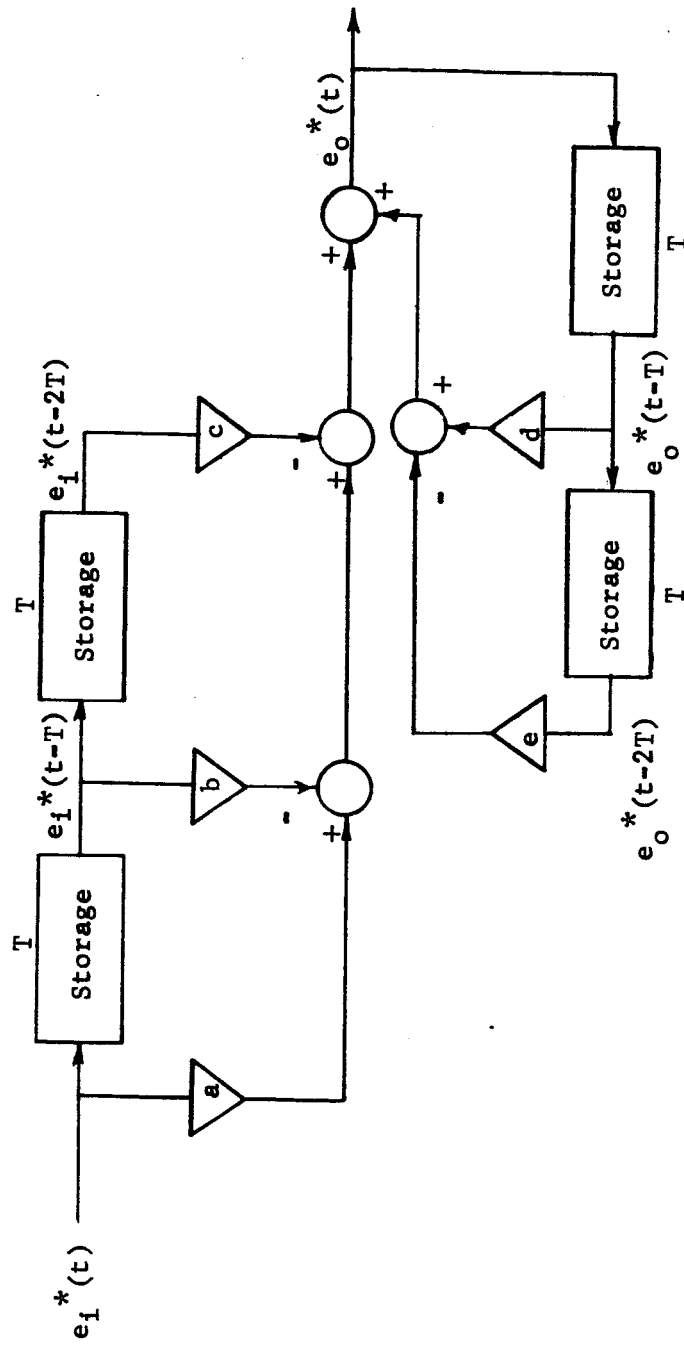
Fig. 20.--Block diagram of direct digital programming of $G_c(z)$.

Frequency (hertz)

a = 0.003125
b = 0.574609
c = 0.590625
d = 1.035936
e = 1.250000

$a_o = a_1 = 0.5$
T = 0.4 seconds
5 term approximation

Fig. 21--Nyquist plot for the ϕ loop alone.

Frequency (hertz)

a = 0.0031
b = 0.4094
c = 0.4594
d = 0.6141
e = 0.8422

$a_o = a_1 = 0.5$
T = 0.4 seconds
5 term approximation

37
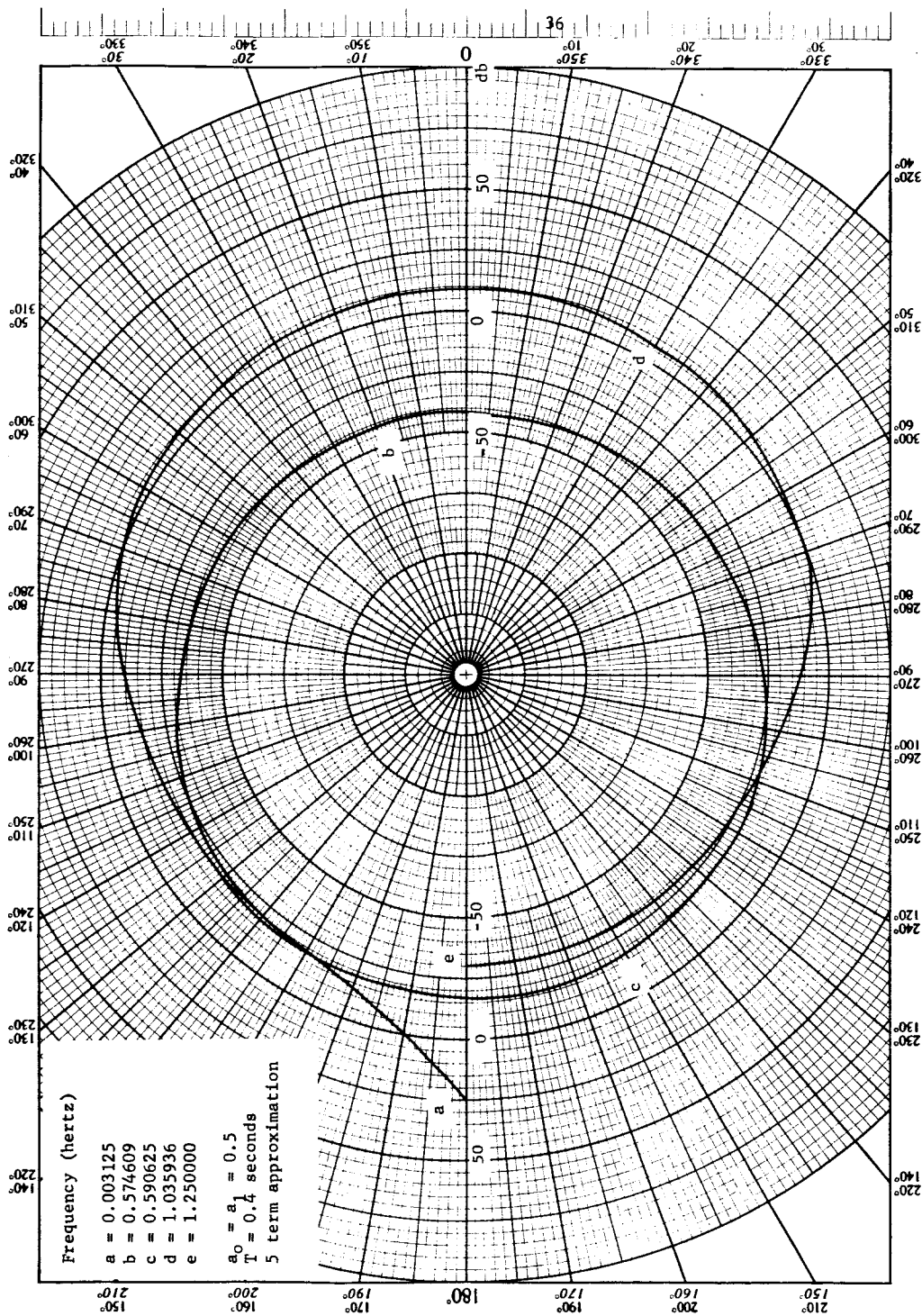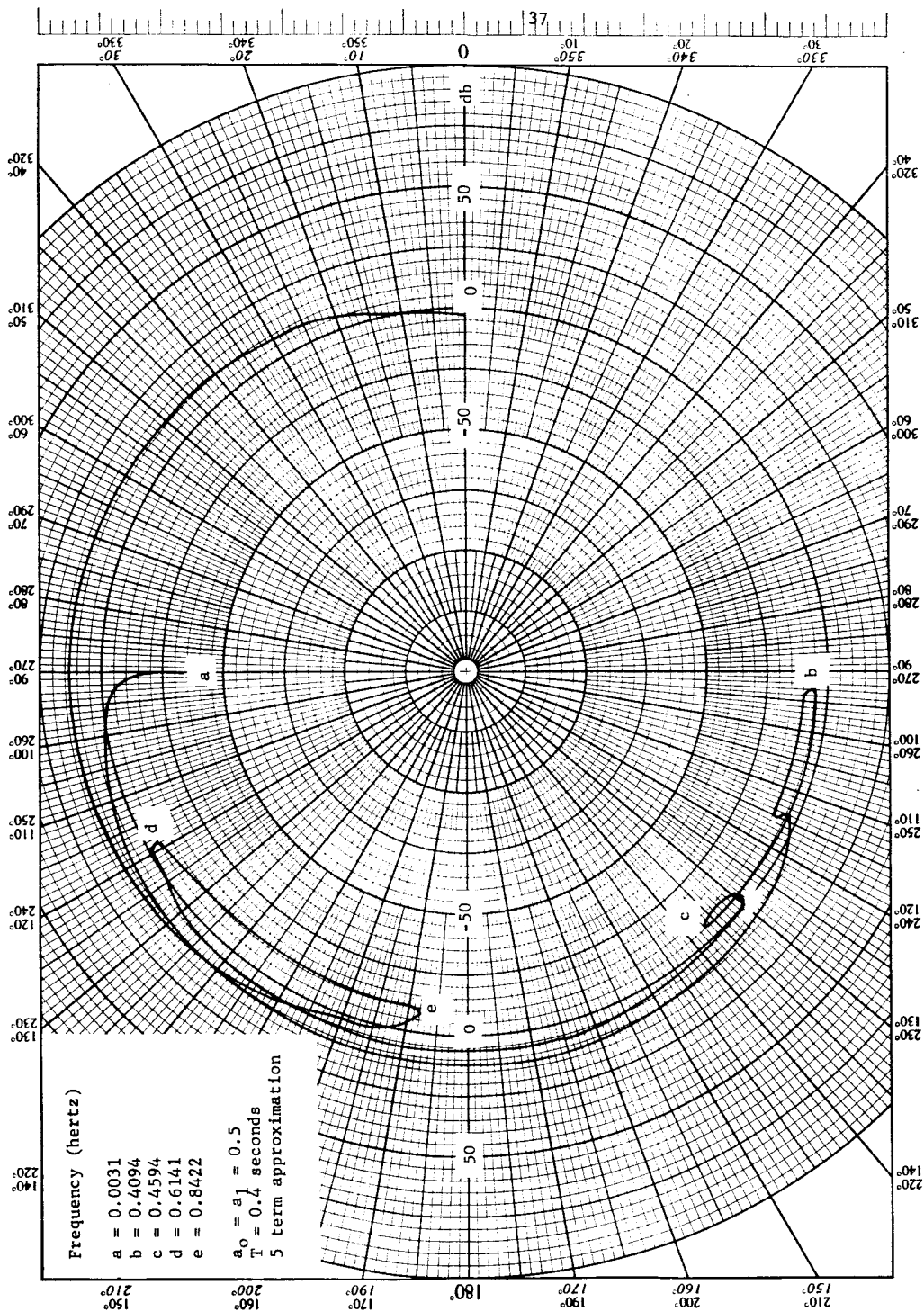
Fig. 22--Nyquist plot for uncompensated system opened in $\dot{\phi}$ channel with ϕ channel closed.
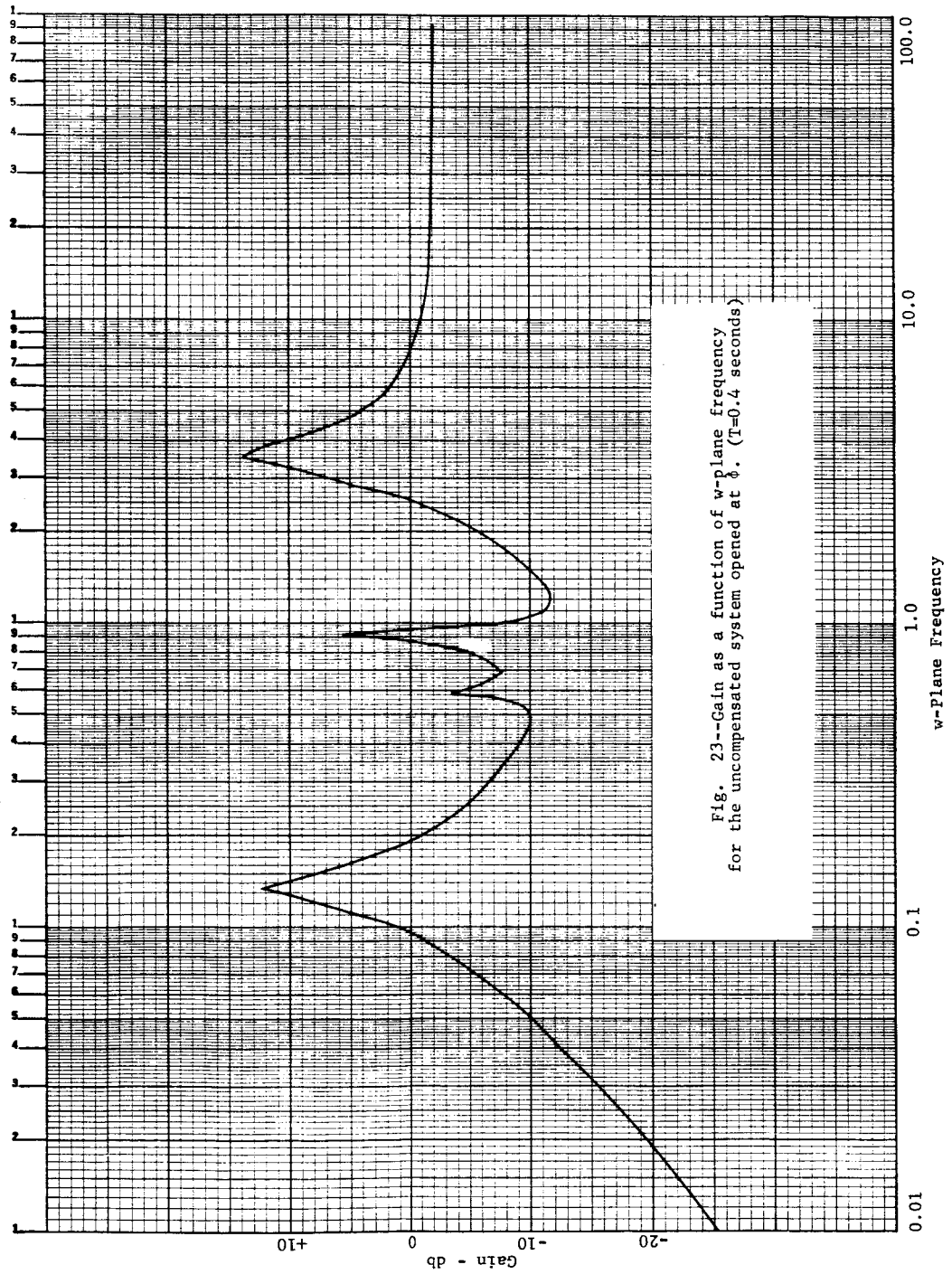
Fig. 23--Gain as a function of w-plane frequency for the uncompensated system opened at ϕ. (T=0.4 seconds).
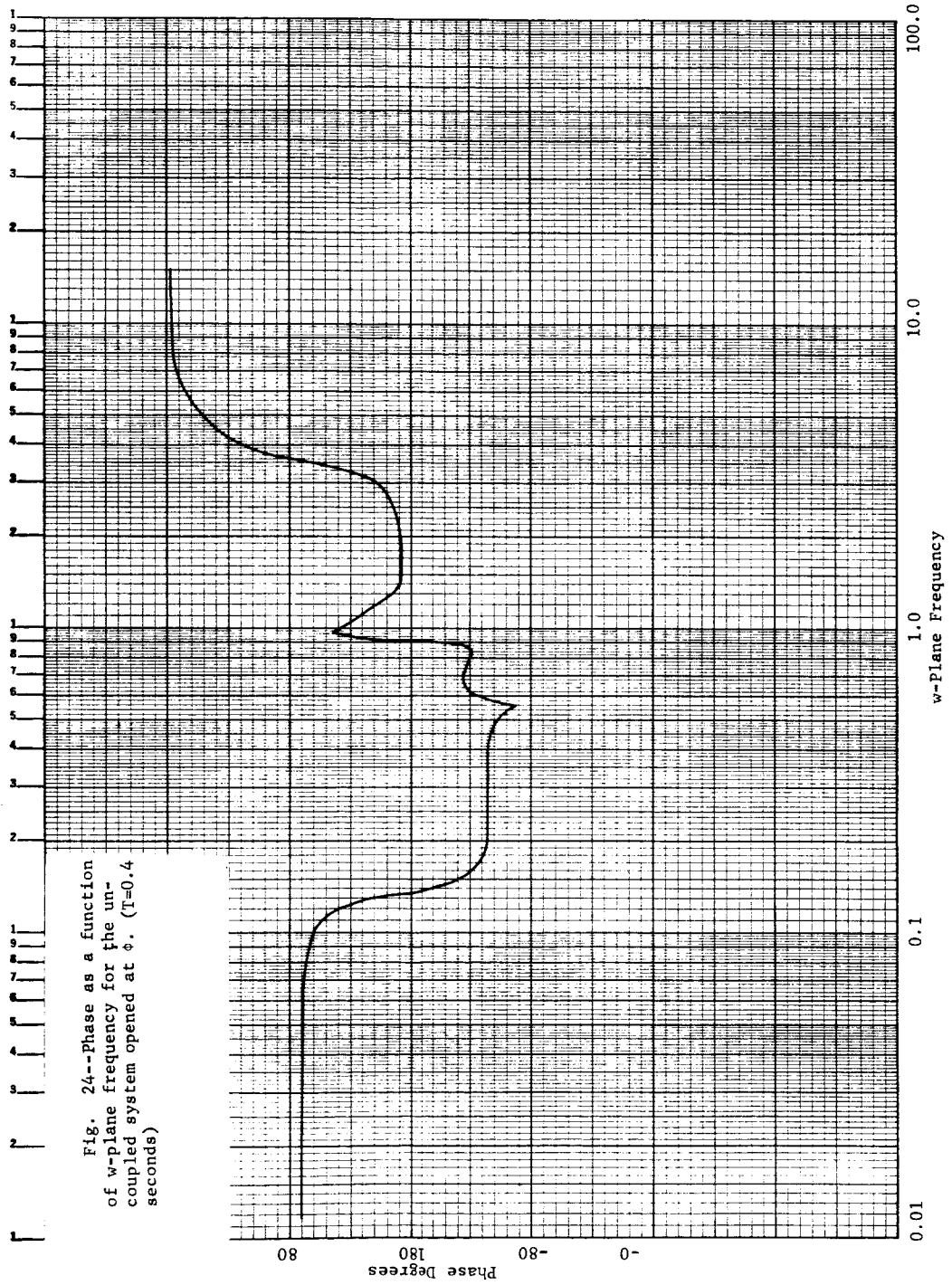
Fig. 24--Phase as a function of w-plane frequency for the un-coupled system opened at φ. (T=0.4 seconds)

$$G_{c1}(w) = \frac{\dfrac{w^2}{(0.92)^2} \quad \dfrac{2(0.5)w}{0.92} + 1}{(\dfrac{w}{0.5} + 1)(\dfrac{w}{0.92} + 1)^2} \tag{20}$$

From Figure 25, which is a Nyquist plot for the compensated

system opened at $\dot{\phi}$, it is seen that $G_{c1}(w)$ stabilizes the system and

provides -30 degrees of phase margin and 11.0 db of gain margin.

Next, in order to more completely evaluate the compensation func-

tion, it is necessary to determine stability margins at ϕ. Figure 26

is a Nyquist diagram for the compensated ϕ loop alone. From this

diagram, it can be determined that the open-loop transfer function

for the thrust vector control system opened at ϕ has one unstable pole.

The Nyquist plot for the compensated system opened in the ϕ channel is

given by Figure 27. The compensated system has -23 degrees of phase

margin and 6 db of gain margin.

The continuous approximation method which was used to derive

stability margins at β_c for the 25 hertz system is not applicable for

the 2.5 hertz system because some of the body-bending frequencies

are greater in magnitude that the sampling frequency.

Although the primary objective of this chapter was to present a

design technique for digital compensation of the T.V.C. System it may

also be observed that the effect of reduced sampling rate is to require

an increase in the complexity of the compensation function in order to

maintain satisfactory stability margins.

Frequency (hertz)

a = 0.0625
b = 0.1450
c = 0.4094
d = 0.4594
e = 0.6141
f = 1.2500

$T = 0.4$
$a_0 = a_1 = 0.5$
5 term approximation

Fig. 25--Nyquist plot for the compensated system opened in the φ loop with the φ loop closed.

Fig. 26--Nyquist plot for the compensated $\dot{\phi}$ loop alone.

Frequency (hertz)

a = 0.0031
b = 0.0312
c = 0.1219
d = 0.2781
e = 1.0119
f = 1.2494

$a_o = a_1 = 0.5$
T = 0.4 seconds
5 term approximation

Fig. 27--Nyquist plot for the compensated system opened in the $\dot{\phi}$ loop with the $\dot{\phi}$ loop closed.

Stability Considerations for
Linear, Sampled-Data Systems

It is well known that a necessary condition for the stability of a sampled data system is that all of the zeroes of the characteristic equation lie within the unit circle of the z-plane. However, the satisfaction of this condition is not sufficient to guarantee that stable behavior will result between sampling instants.

The system response between sampling instants may be determined by application of the modified z-transform technique or other equivalent procedures. The modified z-transform method can provide additional information on system stability which does not result from the equations derived using the standard z-transform method. Additional data is provided if and only if at least one pair of the continuous-data eigenvalues has an imaginary component whose magnitude is $k\omega_s/2$. ω_s is the sampling frequency in radians per second and k is a counting number. The following example is an illustration of this phenomenon.

Consider a continuous data element whose partial fraction expansion is of the form given by equation (21)

$$G(s) = \frac{K_1}{s + \alpha_1} + \cdots\cdots + \frac{K_j}{(s-\sigma)^2 + \omega_s^2} + \cdots\cdots \qquad (21)$$

Taking the z-transform of G(s), we get:

$$G(z) = \mathcal{Z}\left[\frac{K_1}{s + \alpha_1}\right] + \ldots + \mathcal{Z}\left[\frac{K_j}{(s - \sigma)^2 + \omega_s{}^2}\right] \tag{22}$$

The z-transform of the jth term is:

$$\mathcal{Z}\left[\frac{K_j}{(s - \sigma)^2 + \omega_s{}^2}\right] = \frac{2K_j e^{\sigma T}\sin\omega_s T}{\omega_s(z - e^{\sigma T})^2} = 0 \tag{23}$$

Since $\sin \omega_s T = \sin (\frac{2\pi}{T})T = 0$

As a result, the influence of the jth term of (21) on system stability is not considered by a z-transform stability evaluation. Now the modified z-transform of the jth term of (21) does not vanish and is given by (24) below.

$$\mathcal{Z}_m\left[\frac{K_j}{(s - \sigma)^2 + \omega_s{}^2}\right] = \frac{K_j e^{\sigma T}\sin m\omega_s T}{(z - e^{\sigma T})} \tag{24}$$

Let $G_{ij}(s)$ represent the transfer function of the continuous data elements connecting the output of the ith sampler to the input of the jth sampler. Therefore, if any of the $G_{ij}(s)$ has a pole whose imaginary component is equal to $k\omega_s/2$, then there exists a possibility of hidden instability. A more useful assertion is: If none of the $G_{ij}(s)$ has a pole whose imaginary part coincides with $k\omega_s/2$ and if the roots of the system characteristic equation lie within the unit circle, the system is stable.

The preceding discussion indicates that the choice of the system sampling frequency should be based in part on the location of the eigenvalues of the continuous elements of the system. In fact, in the event of poorly defined or slowly varying continuous element parameters, the above arguments lend support to the choice of ω_s such that $\omega_s/2$ is greater than the maximum expected imaginary component of the poles of the $G_{ij}(s)$.

V. ANALYSIS OF MULTIRATE SAMPLED-DATA SYSTEMS

C. L. Phillips

In this chapter various methods of analysis of multirate sampled-data systems are discussed. First a single-loop multirate system is analyzed using the describing-function technique. Then the two techniques presented in STL report No. 4185-6014-RU000, dated 16 April, 1965,[3] are investigated.

Analysis of a Single-Loop Multirate Sampled-Data System

To start the investigation into the methods of analysis of multirate sampled-data control systems, the system of Figure 28 was chosen. This system will be investigated using both the z-transform method and the describing function method.

For the system of Figure 28, the transfer function is seen to be, by the method of switch decomposition,

$$\text{transfer function} = G_1(z)G_2(z) + \sum_{n=1}^{N-1} \left[\epsilon^{\frac{nTs}{N}} G_1(s) \right] \times \tag{25}$$

$$\left[\epsilon^{\frac{nTs}{N}} G_2(s) \right]$$

The switch decomposition method is discussed in the monthly report of 28 November 1964, of this contract. Consider first that N = 2. Then

---

[3]Holzman, op. cit.
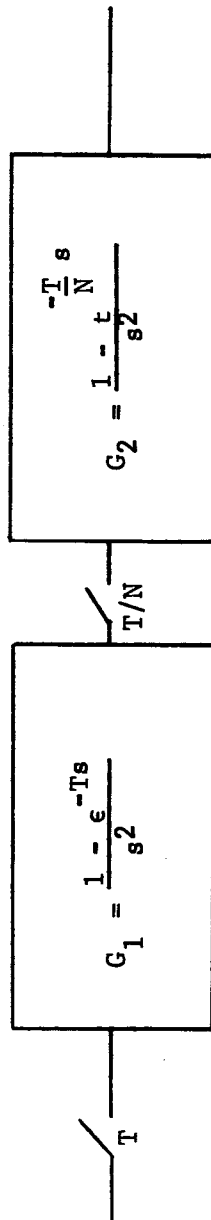
Fig. 28--Multirate sampled-data system.

$$G_1(z) = \frac{T}{z - 1} \qquad (26)$$

$$G_2(z) = \frac{(1/2)T}{z = 1} \qquad (27)$$

$$\mathcal{Z}\left[\epsilon^{\frac{Ts}{2}} G_1(s)\right] = \frac{(1/2)\ T(z + 1)}{(z - 1)} \qquad (28)$$

$$\mathcal{Z}\left[\epsilon^{\frac{-Ts}{2}} G_2(s)\right] = \frac{(1/2)T}{z - 1} \qquad (29)$$

Then

$$\text{transfer function} = \frac{(1/4)T^2\ (z + 3)}{(z - 1)^2} \qquad \bullet \qquad (30)$$

Values of the transfer function are given in Table 1 as z varies along the upper half of the unit circle, for T = 0.04.

The transfer function of (25) can also be written as

$$\text{transfer function} = \left[\frac{1}{T}\sum_{m=-\infty}^{\infty} G_1(s + jm\omega_s)\right]\left[\frac{1}{T}\sum_{m=-\infty}^{\infty} G_2(s+jm\omega_s)\right] \qquad (31)$$

$$+ \sum_{n=1}^{N-1}\left[\frac{1}{T}\sum_{m=-\infty}^{\infty} \epsilon^{\frac{nT}{N}(s+jm\omega_s)} G_1(s+jm_s)\right]\left[\frac{1}{T}\sum_{m=-\infty}^{\infty} \epsilon^{-\frac{nT}{N}(s+jm\omega_s)} GG_2(s+jm\omega_s)\right]$$

TABLE 1

RESPONSE OF SYSTEM OF FIGURE 28 for N = 2

z	$G(z)$	frequency-hz.	describing-function response
$1\angle 15°$	$0.209\angle{-183.9°}$	0.347	$0.209\angle{-183.9°}$
$1\angle 10°$	$0.526 \times 10^{-1}\angle{-188.1°}$	0.694	$0.524\times10^{-1}\angle{-187.9°}$
$1\angle 20°$	$0.1332\times10^{-1}\angle{-195°}$	1.39	$0.130\times10^{-1}\angle{-195.3°}$
$1\angle 50°$	$0.209\times10^{-2}\angle{-218.2°}$	3.47	$0.203\times10^{-2}\angle{-217.5°}$
$1\angle 65°$	$0.1225\times10^{-2}\angle{-230.2°}$	4.51	$0.115\times10^{-2}\angle{-228.7°}$
$1\angle 80°$	$0.806\times10^{-3}\angle{-242.8°}$	5.56	$0.739\times10^{-3}\angle{-240°}$
$1\angle 90°$	$0.635\times10^{-3}\angle{-255.2°}$	6.25	$0.556\times10^{-3}\angle{-247.8°}$
$1\angle 110°$	$0.418\times10^{-3}\angle{-269.90}$	7.65	$0.371\times10^{-3}\angle{-262.5°}$
$1\angle 150°$	$0.235\times10^{-3}\angle{-316.8°}$	10.4	$0.161\times10^{-3}\angle{-292.5°}$
$1\angle 180°$	$0.2\times10^{-3}\angle{0°}$	12.5	$0.934\times10^{-4}\angle{45°}$

If the system is low-pass, then each infinite summation in (31) can be

approximated by the m = 0 term, and the describing-function techni-

que applies. Then (31) becomes

$$\text{transfer function} = \frac{1}{T^2} G_1(s)G_2(s) = \frac{1}{T^2} \sum_{n=1}^{N-1} \left[\epsilon^{\frac{nTs}{N}} G_1(s) \right] \epsilon^{-\frac{nTs}{N}} G_2(s) =$$

$$\frac{N}{T^2} G_1(s)G_2(s) \qquad \bullet \tag{32}$$

For the system of Figure 28, for N = 2,

$$\text{transfer function} = \frac{2}{T^2} \left(\frac{1-\epsilon^{-Ts}}{s^2}\right) \left(\frac{1-\epsilon^{-\frac{Ts}{2}}}{s^2}\right) \qquad \bullet \tag{33}$$

Values of this transfer function are also given in Table 1, with the

s-plane frequencies which correspond to the values of z in the z-plane.

The system of Figure 28 was also investigated for the case that

N = 5. Then

$$\text{transfer function} = G(z)G(z) + \sum_{n=1}^{4} \left[\epsilon^{-\frac{nTs}{5}} G_1(s) \right] \left[\epsilon^{-\frac{nTs}{5}} G_2(s) \right] \qquad \text{,} \tag{34}$$

and

$$G_1(z) = \frac{T}{z-1} \tag{35}$$

$$\mathcal{Z}\left[\epsilon^{\frac{nTs}{5}} G_1(s)\right] = z\left[\frac{\frac{n}{5}T}{z-1} + \frac{T}{(z-1)^2}\right] \tag{36}$$

$$G_2(z) = \frac{(1/2)T}{z-1} \tag{37}$$

$$\mathcal{Z}\left[\epsilon^{\frac{-nTs}{5}} G_2(s)\right] = \frac{(1/5)T}{z-1} \tag{38}$$

Then, from (10),

$$\text{transfer function} = \frac{T^2}{5}\left[\frac{2z + 3}{(z - 1)^2}\right] \tag{39}$$

Using the describing function technique,(31) becomes

$$\text{transfer function} = \frac{5}{T^2} G_1(s)G_2(s) = \frac{5}{T^2}\left(\frac{1-\epsilon^{-Ts}}{s^2}\right)\left(\frac{1-\epsilon^{\frac{-Ts}{5}}}{s^2}\right) \tag{40}$$

Values of the transfer functions (39) and (40) were calculated for values of z and corresponding values of s = jω. These values are given in Table 2.

TABLE 2

RESPONSE OF SYSTEM OF FIGURE 28 for N = 5

z	$G(z)$	frequency-hz.	describing-function response
$1\angle 5°$	$0.211\angle-183.2°$	0.347	$0.210\angle-183.1°$
$1\angle 10°$	$0.526\times10^{-1}\angle-187.7°$	0.694	$0.524\times10^{-1}\angle-189.3°$
$1\angle 20°$	$0.133\times10^{-1}\angle-192°$	1.39	$0.130\times10^{-1}\angle-192°$
$1\angle 50°$	$0.205\times10^{-2}\angle-210.3°$	3.47	$0.203\times10^{-2}\angle-210.3°$
$1\angle 65°$	$0.118\times10^{-2}\angle-219.8°$	4.51	$0.117\times10^{-2}\angle-218.9°$
$1\angle 80°$	$0.754\times10^{-3}\angle-249.5°$	5.56	$0.755\times10^{-3}\angle-228°$
$1\angle 90°$	$0.578\times10^{-3}\angle-236.3°$	6.25	$0.578\times10^{-3}\angle-234°$
$1\angle 110°$	$0.355\times10^{-3}\angle-250.3°$	7.65	$0.384\times10^{-3}\angle-246°$
$1\angle 150°$	$0.139\times10^{-3}\angle 62.3°$	10.4	$0.171\times10^{-3}\angle 90°$
$1\angle 180°$	$0.8\times10^{-4}\angle 0°$	12.5	$0.102\times10^{-3}\angle 72°$

For the system described above, one sampler operated at 25 cps and the other at either 50 cps or 125 cps. In either case, the describing-function approach is limited to frequencies less than $f_s/2$, or 12.5 cps, since an input frequency of greater than $f_s/2$ will generate a reflected frequency at less than $f_s/2$. It is seen from Table 1 and Table 2 that good correlation is obtained between the z-transform approach and the describing-function approach for frequencies less than $f_s/2$. It is noted that better correlation is obtained for frequencies much less than $f_s/2$ than for frequencies in the neighborhood of $f_s/2$.

Multirate Analysis Technique No. 2

The first method of analysis of the aforementioned STL report to be investigated is Technique No. 2. This method is based on switch decomposition. It will be shown that one of the results obtained in the STL report is in error.

Technique No. 2 is a method of finding the characteristic equation of a multirate sampled-data control system. The system considered here will have a definite relationship between the different sampling rates, but the method used can be applied to any multirate system for which the ratio of the sampling rates is the ratio of two integers.

Consider the system of Figure 29. One sampler operates at a rate of T/2 and the other at a rate of T/3. Using the switch-decomposition method, the system can be redrawn as shown in Figure 30. The charac-

For the system described above, one sampler operated at 25 cps and the other at either 50 cps or 125 cps. In either case, the describing-function approach is limited to frequencies less than $f_s/2$, or 12.5 cps, since an input frequency of greater than $f_s/2$ will generate a reflected frequency at less than $f_s/2$. It is seen from Table 1 and Table 2 that good correlation is obtained between the z-transform approach and the describing-function approach for frequencies less than $f_s/2$. It is noted that better correlation is obtained for frequencies much less than $f_s/2$ than for frequencies in the neighborhood of $f_s/2$.

Multirate Analysis Technique No. 2

The first method of analysis of the aforementioned STL report to be investigated is Technique No. 2. This method is based on switch decomposition. It will be shown that one of the results obtained in the STL report is in error.

Technique No. 2 is a method of finding the characteristic equation of a multirate sampled-data control system. The system considered here will have a definite relationship between the different sampling rates, but the method used can be applied to any multirate system for which the ratio of the sampling rates is the ratio of two integers.

Consider the system of Figure 29. One sampler operates at a rate of T/2 and the other at a rate of T/3. Using the switch-decomposition method, the system can be redrawn as shown in Figure 30. The charac-

Fig. 29 --Single-loop multirate sampled-data system.
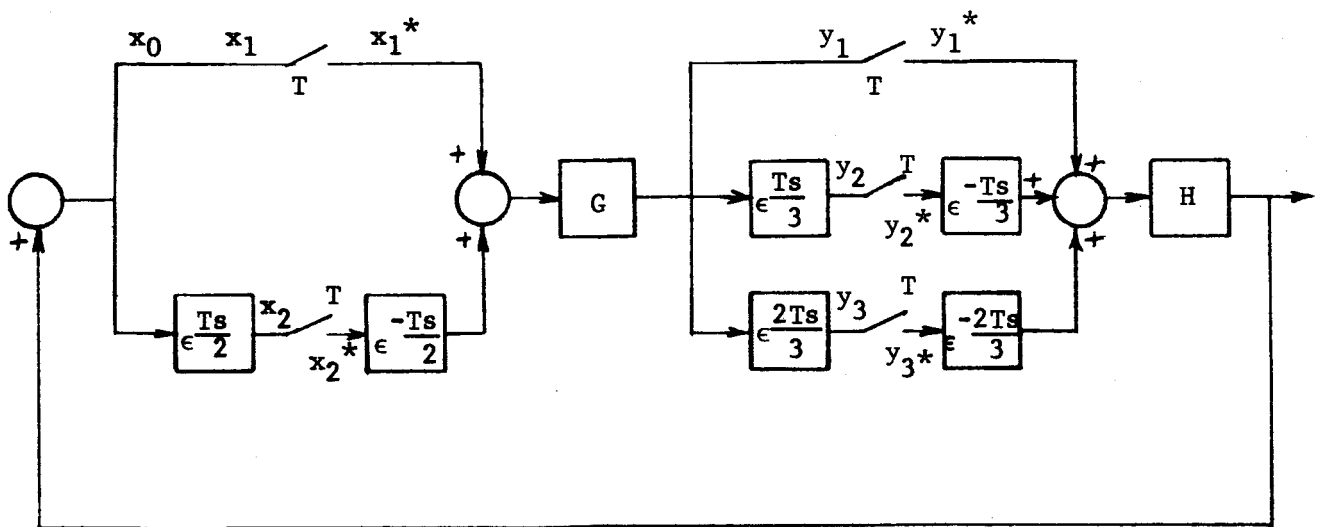
Fig. 30 --System equivalent to that of Figure 29.

teristic equation can be found by opening a loop in front of any of the samplers, writing the open-loop transfer function, and setting this transfer function equal to one.

Suppose that the system of Figure 30 is opened at the point $x_0 - x_1$, and let x_0 be the output and x_1 be the input. Then the following equations can be written.

$$y_1^* = G^* x_1^* + (G\epsilon^{-\frac{Ts}{2}})^* x_2^*$$

$$y_2^* = (\epsilon^{\frac{Ts}{3}} G)^* x_1^* + (\epsilon^{-\frac{Ts}{2}})^* x_2^* \qquad (41)$$

$$y_3^* = (\epsilon^{\frac{2Ts}{3}} G)^* x_1^* + (\epsilon^{\frac{2Ts}{3}} G\epsilon^{-\frac{Ts}{2}})^* x_2^*$$

and

$$x_0^* = H^* y_1^* + (H\epsilon^{-\frac{Ts}{3}})^* y_2^* + (h\epsilon^{-\frac{2Ts}{3}})^* y_3^*$$

$$\qquad (42)$$

$$x_2^* = (\epsilon^{-\frac{Ts}{2}} H)^* y_1^* + (\epsilon^{\frac{Ts}{2}} H\epsilon^{-\frac{Ts}{3}})^* y_2^* + (\epsilon^{\frac{Ts}{2}} H\epsilon^{-\frac{2Ts}{3}})^* y_3^*$$

In vector-matrix notation, (41) and (42) can be expressed as, respectively,

$$\underline{y}^* = A\underline{x}^* \qquad (43)$$

$$\begin{bmatrix} x_0{}^* \\ x_2{}^* \end{bmatrix} = B\underline{y}^* \tag{44}$$

To simplify the notation, let

$$(\epsilon^{\frac{(i-1)Ts}{3}} G \epsilon^{-\frac{(j-1)Ts}{2}})^* = g_{ij} \tag{45}$$

and

$$(\epsilon^{\frac{(i-1)Ts}{2}} H \epsilon^{-\frac{(j-1)Ts}{3}})^* = h_{ij} \tag{46}$$

Then A and B can be expressed as

$$A = \begin{bmatrix} g_{11} & g_{12} \\ g_{21} & g_{22} \\ g_{31} & g_{32} \end{bmatrix} , \qquad B = \begin{bmatrix} h_{11} & h_{12} & h_{13} \\ h_{21} & h_{22} & h_{23} \end{bmatrix}$$

Then (43) and (44) can be expressed as

$$\begin{bmatrix} x_0{}^* \\ x_2{}^* \end{bmatrix} = B\underline{y}^* = BA\underline{x}^* = C\underline{x}^* \tag{47}$$

where

$$C = \begin{bmatrix} h_{11}g_{11} + h_{12}g_{21} + h_{13}g_{31} & h_{11}g_{12} + h_{12}g_{22} + h_{13}g_{32} \\ h_{21}g_{11} + h_{22}g_{21} + h_{23}g_{31} & h_{21}g_{12} + h_{22}g_{22} + h_{23}g_{32} \end{bmatrix} \quad (48)$$

Let

$$c_{ij} = \sum_{n=1}^{3} h_{in}g_{nj} \quad (49)$$

Then (48) becomes

$$C = \begin{bmatrix} c_{11} & c_{12} \\ c_{21} & c_{22} \end{bmatrix} \quad (50)$$

and, from (47),

$$\begin{bmatrix} x_0{}^* \\ x_2{}^* \end{bmatrix} = \begin{bmatrix} c_{11} & c_{12} \\ c_{21} & c_{22} \end{bmatrix} \begin{bmatrix} x_1{}^* \\ x_2{}^* \end{bmatrix} \quad (51)$$

or

$$x_0{}^* = \left[\frac{c_{11}(c_{22} - 1) - c_{12}c_{21}}{c_{22} - 1} \right] x_1{}^* \quad (52)$$

The characteristic equation, obtained by setting the expression in brackets in (52) equal to 1, is

$$(c_{11} - 1)(c_{22} - 1) - c_{12}c_{21} = 0 \tag{53}$$

or

$$1 - c_{11} - c_{22} + c_{11}c_{22} - c_{12}c_{21} = 0 \tag{54}$$

From (49), (54) becomes

$$1 - \sum_{n=1}^{3} h_{1n}g_{n1} - \sum_{n=1}^{3} h_{2n}g_{n2} \sum_{n=1}^{3} h_{1n}g_{n1} \sum_{n=1}^{3} h_{2n}g_{n2}$$

$$- \sum_{n=1}^{3} h_{1n}g_{n2} \sum_{n=1}^{3} h_{2n}g_{n1} = 0 \tag{55}$$

From (45) and (46), (55) becomes

$$1 - \sum_{n=1}^{3} (He^{\frac{-(n-1)Ts}{3}})*(e^{\frac{(n-1)Ts}{3}} \cdot G)* - \sum_{n=1}^{3} (e^{\frac{Ts}{2}} He^{\frac{-(n-1)Ts}{3}})*$$

$$(e^{\frac{(n-1)Ts}{3}} G e^{\frac{-Ts}{2}})* \qquad \text{(continued)}$$

$$+ \sum_{n=1}^{3} (H\epsilon^{\frac{-(n-1)Ts}{3}})^* (\epsilon^{\frac{(n-1)Ts}{3}}G)^* \sum_{n=1}^{3} (\epsilon^{\frac{-(n-1)Ts}{3}})^* (\epsilon^{\frac{(n-1)Ts}{3}}G\epsilon^{\frac{-Ts}{2}})^*$$

$$- \sum_{n=1}^{3} (H\epsilon^{\frac{-(n-1)Ts}{3}})^* (\epsilon^{\frac{(n-1)Ts}{3}}G\epsilon^{\frac{-Ts}{2}}) \sum_{n=1}^{3} (\epsilon^{\frac{Ts}{2}}H\epsilon^{\frac{-(n-1)Ts}{3}})^* (\epsilon^{\frac{(n-1)Ts}{3}}G)^* = 0 \tag{56}$$

It will be noted that this equation is different from the characteristic equation obtained from Equation (2.84) of the STL report. This equation is

$$1 - \sum_{m=1}^{P} \sum_{n=1}^{q} \left[\epsilon^{\frac{-(m-1)Ts}{P}} \epsilon^{\frac{(n-1)Ts}{q}} G(s) \right] \left[\epsilon^{\frac{-(n-1)Ts}{q}} \epsilon^{\frac{(m-1)Ts}{P}} H(s) \right] = 0 \tag{57}$$

where one sampling rate is T/p and the other is T/q. For the example, p was 2 and q was 3. All of the terms of (57) are included in (56), but terms appear in (56) which do not appear in (57).

It is seen that difficulties will occur if (56) is used to obtain a Nyquist diagram in order to determine the gain margin and phase margin with respect to either G or H. These difficulties arise from the presence of terms in (56) which will result in the gain of both G and H appearing in squared form.

The method illustrated here is also applicable to multirate

multiloop sampled-data systems. Each sampler should be replaced by a parallel combination of samplers, as shown in Figure 30. Then, by opening the system in front of any sampler, an open-loop transfer function can be obtained. However, this transfer function would not have any physical meaning.

Multirate Analysis Technique No. 1

The multirate analysis Technique No. 1 of the aforementioned STL report was investigated, and the final result, given by equation (2.73) of the report, was found to be correct. However, some of the steps in the analysis are not clear, and these steps are discussed below.

To be mathematically correct, in equation (2.45) and (2.46) the factor $\delta(n-kN)$ should be replaced by

$$\int_{n-\epsilon}^{n+\epsilon} \delta(n-kN)dn \qquad \epsilon > 0 \quad ,$$

since this integral is equal to unity for n = kN, and is zero for all other values of n.

The motivation behind the substitution

$$x(n) = \frac{1}{N} \sum_{m=1}^{N} \epsilon^{j\frac{2\pi mn}{N}} = \frac{1}{N} \sum_{r=\alpha}^{N+\alpha-1} \epsilon^{j\frac{2\pi rn}{N}} \tag{58}$$

obtained from (2.51) and (2.53), is obscure and the substitution seems
to be unnecessary. The summation in the above equation, from α to
($N+\alpha-1$), is carried through the derivation intact. Then, in equation
(2.69), this summation is replaced with a summation from 1 to N,
which is the original summation in (58).

It is seen, from (2.74), that the same problems arise in using
Technique No. 1 as in using Technique No. 2. Using both techniques,
the gain factor K cannot be factored from the open loop transfer
functions, and thus gain and phase margins cannot be obtained in a
simple manner from a Nyquist diagram of the system.

VI. CONCLUSIONS

In Chapter II, a method was discussed by which one can determine the exact gain and phase margin in any channel of a multiloop, single rate, sampled-data system. This "exact method" was found to be rather unwieldy in application. Further, it does not enable one to compute an open-loop frequency response for the system opened between continuous elements and is therefore of little value in the synthesis of a compensation function.

The influence of a reduced sampling rate on the configuration described by Figure 1 was investigated in Chapter III. The system was found to be stable for a sampling rate of 2.5 hertz although the rigid body stability margins are decreased relative to the same margins for the 25 hertz rate. It was also noted that the reduced sampling rate suppressed appreciably the bending mode resonances and thereby minimized the effect of these modes on stability.

A technique was presented in Chapter IV which enables the systematic development and evaluation of a compensation function for the thrust vector control system with synchronous, equal rate, sampling in each of the attitude and rate channels. The technique was illustrated by example with the development of compensation functions for each of the 2.5 hertz and 25 hertz sampling rates. The problem of "hidden instability" was also discussed and a method of assuring that the system is stable between sampling instants was presented.

In Chapter V, the describing function method was applied to a
single loop, multi-rate system. Also a study was conducted of two
techniques for the analysis of multi-loop, multi-rate sampling systems.
These techniques were described in STL report no. 4185-6014-RU00,
dated 16 April, 1965

The following is a list of the transfer functions used in the body of the report.

$$G1R = \frac{-0.94068468}{s^2 - 0.02972784}$$

$$G1B1 = \frac{0.65323138 \times 10^{-2}(s^2 + 498.59362)}{s^2 + 0.64905305 \times 10^{-1}s + 42.126986}$$

$$G1B2 = \frac{-0.40378959 \times 10^{-2}(s^2 + 485.48033)}{s^2 + 0.1201345s + 144.32299}$$

$$G1B3 = \frac{-0.53896739 \times 10^{-2}(s^2 + 470.36052)}{s^2 + 0.18378317s + 337.76255}$$

$$G1B4 = \frac{0.58368238 \times 10^{-2}(s^2 + 469.03256)}{s^2 + 0.22481237s + 505.40603}$$

$$G_2 = s(G1R + G1B1 + G1B2 + G1B3 + G1B4) = s\ G_1$$

$$W_{ss} = \frac{625.0}{s^2 + 25.0s + 625.0}$$

$$HOL = \frac{1 - e^{-(T)s}}{s}$$

$$PHDTCO = \left[\frac{0.33747 \times 10^{-8}s^8 + 0.57852 \times 10^{-7}s^7}{0.31188 \times 10^{-10}s^9 + 0.30536 \times 10^{-7}s^8} \right.$$

$$+ \frac{0.32159 \times 10^{-5}s^6 + 0.38442 \times 10^{-4}s^5 + 0.727818 \times 10^{-3}s^4}{0.13131 \times 10^{-5}s^7 + 0.33399 \times 10^{-4}s^6 + 0.59308 \times 10^{-3}s^5}$$

$$+ \frac{0.0069727s^3 + 0.55606s^2 + 0.38360s + 1.0}{0.0068924s^4 + 0.056518s^3 + 0.30188s^2 + 0.87623s + 1.0}$$

GENERALIZED NYQUIST PROGRAM FOR SYSTEM OPENED AT ϕ.

```
C     *****************************
C         NYQ DIAGRAM - SERIES EXP METHOD
C     *****************************
C         BROKEN IN PHI CHANNEL
C     *****************************
 1  10 FORMAT(5(5X,E15.8))
 2  20 FORMAT(7X,92HFREQ(HERTZ)        FREQ(RADIANS)           MAGNITUDE
    1         MAGNITUDE IN DB         ANGLE IN DEG,//)
 3  30 FORMAT(1H1)
 4     PIE = 3.1415926
 5     COMPLEX S,HELP,THTA1,THTA2,G1,G1R,G1B1,G1B2,G1B3,G1B4,G2,WSS,
    1PHDTCO,HUL,C(5)
 6  40 FORMAT(3(5X,E15.8))
 7  41 FORMAT(5X,I1)
10  97 READ (5,40) T, A2, A1
11     READ (5,40) XO1, XO2, GAIN
12     READ (5,41) KCOMP
14  50 FORMAT(6(3X,E15.8),(7X,I1),//)
15  60 FORMAT(3X,118HSAMPLE TIME-SEC        THTA1-RAD          THTA2-RAD
    1      THTA1-RAD          THTA2-RAD        A(2)      A(1)      KCOMP
    2,//)
16     PRINT 60
17     PRINT 50, T,A2,A1,XO1,XO2,GAIN,KCUMP
20     THTA1 = CMPLX(0.0,XO1)
21     THTA2 = CMPLX(0.0,XO2)
22     PRINT 20
```

DIGITAL COMPUTER PROGRAM
(continued)

```
23        WS = (2.0*PIE)/T
24        WT = 0.00125 * WS
25        WL = WS/2.0
26        W = 0.00
27     1  W = W + 0.00125 * WS
30        WM = W - 0.00125 * WS
31        GO TO 61
32    62  W = (WM + W)/2.0
33    61  S = CMPLX(0.0,W)
34        C(4) = (0.0, 0.0)
35        DO 98 J = 1,9
36        N = -5 + J
37        XN = N
40        W1 = W +XN*WS
41        S = CMPLX(0.0,W1)
42        G1R = (-0.94068468,0.0)/(S**2 + (-0.029772784,0.0))
43        G1B1 = (0.65323138E-02)*(S**2 + (498.59362,0.0))/
         1(S**2+(0.64905305E-01)*S+(42.126986,0.0))
44        G1B2 = -(0.40378959E-02)*(S**2+(485.48033,0.0))/
         1(S**2 + 0.1201345*S + (144.32299,0.0))
45        G1B3 = - (0.53896739E-02)*(S**2+ (470.36052,0.0))/
         1(S**2+0.18378317*S + (337.76255,0.0))
46        G1B4 = (0.58368238E-02)*(S**2 + (469.03256,0.0))/
         1(S**2 + 0.22481237*S + (505.40603,0.0))
47        G1 = G1R + G1B1 + G1B2 + G1B3 + G1B4
50        G2 = S*G1
51        WSS = (625.0,0.0)/(S**2 + 25.0*S + (625.0,0.0))
52        HOL = ((1.0,0.0) -CEXP(-T*S))/S
```

DIGITAL COMPUTER PROGRAM
(continued)

```
53        IF (KCOMP.EQ.1) GO TO 99
56        C(3) = (1.0/T)*(A1*GAIN*CEXP(THTA1)*HUL*WSS*G1)/((1.0,0.0) -
          1(GAIN*A2*CEXP(THTA1)*CEXP(THTA2)*WSS*G2))
57        GO TO 98
60    99  PHDTCO = ((0.33747E-08)*S**9+(0.57852E-07)*S**7+(0.32159E-05)*S**6
          1+(0.38442E-04)*S**5+(0.727818E-03)*S**4+(0.0069727)*S**3
          2+(0.055606)*S**2+0.38360*S+(1.0,0.0))/((0.31188E-10)*S**9+
          3(0.30536E-07)*S**8+(0.13131E-05)*S**7+(0.33399E-04)*S**6+
          4(0.59308E-03)*S**5+0.0068924*S**4+0.056518*S**3+0.30188*S**2+
          50.87623*S+(1.0,0.0))
61        C(3) = (1.0/T)*(A1*GAIN*CEXP(THTA1)*HUL*WSS*G1)/((1.0,0.0) -
          1(GAIN*A2*CEXP(THTA1)*CEXP(THTA2)*WSS*G2*PHDTCO))
62    98  C(4) = C(4) + C(3)
64        HELP = -C(4)
65        XREAL = REAL(HELP)
66        XIMAG = AIMAG(HELP)
67        XMAG = SQRT(XREAL**2 +XIMAG**2)
70        ANGLE = ATAN(XIMAG/XREAL)
71        IF(XREAL.EQ.0.0) IF(XIMAG) 3,4,5
74        IF(XREAL.GT.0.0) GO TO 6
77        IF(XREAL.LT.0.0) IF(XIMAG) 2,2,8
102   8   ANGLE = ANGLE + PIE
103       GO TO 6
104   2   ANGLE = ANGLE - PIE
105       GO TO 6
106   3   ANGLE = -PIE/2.0
107   4   GO TO 6
```

DIGITAL COMPUTER PROGRAM
(continued)

```
110    5 ANGLE = PIE/2.0
111    6 ANGLE = ANGLE*180.0/PIE
112      FREQ = W/(2.0*PIE)
113      DB = 20.0*ALOG10(XMAG)
114      IF (ANGLE.LT.0.0) GO TO 65
117      ROTAT = ANGLE
120      GO TO 66
121   65 ROTAT = ANGLE + 360.0
122   66 IF(W.EQ.WT) GO TO 63
125      DELTA = ABS(PHASE - ROTAT)
126      IF(DELTA.GT.180.0) GO TO 71
131      GO TO 72
132   71 DELTA = 360.0 - DELTA
133   72 IF(DELTA.GT.15.0) GO TO 62
136   63 PHASE = ROTAT
137   64 DBP = DB
140      PRINT 10,FREQ,W,XMAG,DBP,ANGLE
141      IF(W-WL) 1,1,96
142   96 PRINT 30
143      GO TO 97
144      END
```

APPENDIX C

EXAMPLE OF DIGITAL COMPUTER PROGRAM USED TO DETERMINE
NYQUIST DIAGRAMS FOR THE DIGITAL COMPENSATION OF THE TVC SYSTEM

```
      ********************************
      NYQ DIAGRAM - SERIES EXP METHOD
      ********************************
10    FORMAT(5(5X,E15.8))
20    FORMAT(7X,92HFREQ(HERTZ)        FREQ(RADIANS)           WFREQ
     1          MAGNITUDE IN DB        ANGLE IN DEG.//)
30    FORMAT(1H1)
40    FORMAT((5X,F15.8),(5X,I2),(3X,I1),//)
50    FORMAT(5X,27HSAMPLE TIME-SEC      K      KW,//)
60    FORMAT(5X,F15.8)
70    FORMAT((5X,F15.8),(5X,I2),(3X,I1))
      COMPLEX S,R,HELP,G1,G1R,G1B1,G1B2,G1B3,G1B4,G2,HOL,C(9),WSS,GC,GA
     1 , CMPLX , CEXP,P
      PIE = 3.1415926
97    READ(5,70) T, K, KW
      PRINT 50
      PRINT 40, T, K, KW
      PRINT 20
      WS = (2.0*PIE)/T
      WT = 0.00125 * WS
      WL = WS/2.0
      WA = 0.0025*WS
      W3 = 40.0
      W = 0.00
      IF(KW.EQ.1) GO TO 12
```

C
C
C

DIGITAL COMPUTER PROGRAM
(continued)

```
   1 W = W + 0.00125 * WS
     WM = W - 0.00125 * WS
     GO TO 61
  41 W = W + 0.0125*WS
     WM = W - 0.0125*WS
     GO TO 61
  62 W = (WM + W)/2.0
     GO TO 61
  12 READ (5,60) W2
     WT = ABS(SQRT(W2))
     W = WT
  61 S = CMPLX(0.0,W)
     R = (CEXP(T*S) - 1.0)/(CEXP(T*S) + 1.0)
     WFREQ = AIMAG(R)
     C(6) = (0.0,0.0)
     C(4) = (0.0, 0.0)
     DO 98 J = 1,K
     I = -(K+1)/2
     N = I + J
     XN = N
     W1 = W +XN*WS
     S = CMPLX(0.0,W1)
     G1R = (-0.94068468,0.0)/(S**2 + (-0.029727784,0.0))
     G1B1 = (0.65323138E-02)*(S**2 + (498.59362,0.0))/
    1(S**2+(0.64905305E-01)*S+(42.126986,0.0))
     G1B2 = -(0.40378959E-02)*(S**2+(485.48033,0.0))/
    1(S**2 + 0.1201345*S + (144.32299,0.0))
     G1B3 = - (0.53896739E-07)*(S**2+ (470.36052,0.0))/
```

DIGITAL COMPUTER PROGRAM
(continued)

```
1(S**2+0.18378317*S + (337.76255,0.0))
G1B4 = (0.58368238E-02)*(S**2 + (469.03256,0.0))/
1(S**2 + 0.22481237*S + (505.40603,0.0))
G1 = G1R + G1B1 + G1B2 + G1B3 + G1B4
G2 = S*G1
WSS = (625.0,0.0)/(S**2 + 25.0*S + (625.0,0.0))
HOL = ((1.0,0.0) -CEXP(-T*S))/S
C(3) = G2 * HOL * WSS/(2.0*T)
C(5) = G1 * HOL * WSS/(2.0 * T)
C(6) = C(6) + C(5)
C(4) = C(4) + C(3)
98 P = CMPLX(0.0,WFREQ)
GC = (17.361111*P**2 + 2.0833333*P + (1.0,0.0))/((14.285714*P +
1(1.0,0.0))*(14.285714*P + (1.0,0.0)))
GA = -(C(4) * GC + C(6))
XREAL = REAL(GA)
XIMAG = AIMAG(GA)
XMAG = SQRT(XREAL**2 +XIMAG**2)
ANGLE = ATAN(XIMAG/XREAL)
IF(XREAL.EQ.0.0) IF(XIMAG) 3,4,5
IF(XREAL.GT.0.0) GO TO 6
IF(XREAL.LT.0.0) IF(XIMAG) 2,2,8
8 ANGLE = ANGLE + PIE
GO TO 6
2 ANGLE = ANGLE - PIE
GO TO 6
3 ANGLE = -PIE/2.0
4 GO TO 6
```

DIGITAL COMPUTER PROGRAM
(continued)

```
 5   ANGLF = PIF/2.0
 6   ANGLE = ANGLE*180.0/PIF
     FREQ = W/(2.0*PIE)
     DB = 20.0*ALOG10(XMAG)
     IF (ANGLF.LT.0.0) GO TO 65
     ROTAT = ANGLE
     GO TO 66
65   ROTAT = ANGLE + 360.0
66   IF(W.EQ.WT) GO TO 63
14   DELTA = ABS(PHASF - ROTAT)
     IF(DELTA.GT.180.0) GO TO 71
     GO TO 72
71   DELTA = 360.0 - DELTA
72   IF(DELTA.GT.15.0) GO TO 62
63   PHASE = ROTAT
64   DBP = DB
     PRINT 10, FREQ, W, WFREQ, DBP, ANGLE
     IF(WT.GT.WA) GO TO 12
     IF(W.GT.WL) GO TO 96
     IF(W.GT.W3) GO TO 41
     IF(W-WL) 1,1,96
96   PRINT 30
     GO TO 97
     END
```